BMI-1730

[redacted]

HIGH-TEMPERATURE IRRADIATION OF NIOBIUM-1 w/o ZIRCONIUM-CLAD UO_2

AEC RESEARCH AND DEVELOPMENT REPORT

BATTELLE MEMORIAL INSTITUTE

DISCLAIMER

[redacted]

Report No. BMI-1730

[redacted] Advanced Concepts for Future Application-Reactor Experiments [redacted]

UNCLASSIFIED

AEC Contract W-7405-eng-92

[redacted]

HIGH-TEMPERATURE IRRADIATION OF NIOBIUM-1 w/o ZIRCONIUM-CLAD UO_2

BMI--1730

DE86 000993

by

Mihkel Kangilaski
Earle O. Fromm
Donald H. Lozier
Victor W. Storhok
John E. Gates

June 28, 1965

[redacted]

MASTER

BATTELLE MEMORIAL INSTITUTE
505 King Avenue
Columbus, Ohio 43201

[redacted]

[redacted]

TABLE OF CONTENTS

	Page
ABSTRACT	1
INTRODUCTION	1
EXPERIMENTAL PROGRAM	1
COMPATIBILITY STUDIES	3
UO_2-Lithium	3
UO_2-Lithium-Niobium-1 w/o Zirconium	4
Lithium-Niobium-1 w/o Zirconium	6
CAPSULE DESIGN	6
SPECIMEN DESIGN AND FABRICATION	6
Fuel-Pellet Fabrication	10
Specimen Cladding	10
IRRADIATION HISTORY	13
POSTIRRADIATION EXAMINATION	16
Capsule Opening	16
Dimensional Measurements	17
Gamma Scanning	17
Burnup Determinations	20
Fission-Gas Release	22
Metallographic Examination	25
Oxygen/Uranium Ratio of UO_2	47
CONCLUSIONS	49
REFERENCES	50
APPENDIX A	
CLADDING DESIGN CRITERIA	A-1
APPENDIX B	
BURNUP ANALYSES	B-1
APPENDIX C	
FISSION-PRODUCT-OXIDE FORMATION	C-1

[redacted]

UNCLASSIFIED

[redacted]

HIGH-TEMPERATURE IRRADIATION OF NIOBIUM-1 w/o ZIRCONIUM-CLAD UO_2

Mihkel Kangilaski, Earle O. Fromm, Donald H. Lozier, Victor W. Storhok, and John P. Gates

Twenty-four 0.225-in.-diameter and six 0.290-in.-diameter UO_2 specimens clad with 80 mils of niobium-1 w/o zirconium were irradiated to burnups of 1.4 to 6.0 a/o of uranium at surface temperatures of 900 to 1400 C. UO_2 and lithium were found to be incompatible at these temperatures and the thick cladding was used primarily to minimize the chances of contact of UO_2 and the lithium coolant. The thickly clad specimens did not undergo any dimensional changes as a result of irradiation, although it was found that movement of UO_2 took place in the axial direction by a vaporization-redeposition mechanism. It was found that 32 to 87 per cent of the fission gases was released from the fuel, depending on the temperature of the specimen.

Metallographic examination of longitudinal and transverse sections of the specimens indicated the usual UO_2 microstructure with columnar grains. Grain-boundary thickening was observed in the UO_2 at higher burnups. The oxygen/uranium ratio of UO_2 increased with increasing burnup.

INTRODUCTION

In the past decade, UO_2 has become the mainstay nuclear fuel in pressurized- and boiling-water reactors. Uranium dioxide has demonstrated good dimensional stability during irradiation and it is compatible with almost all cladding materials. Recently, UO_2 has been irradiated at more stringent heat ratings[1]*. Because of its good compatibility with cladding materials at high temperatures, it was decided to consider UO_2 as a possible fuel for compact reactors such as SNAP-50. Although preliminary tests showed that UO_2 was incompatible with lithium at 1200 C, which is the coolant for SNAP-50, it was decided to irradiate UO_2 at SNAP-50 operating conditions. To eliminate specimen failures which would result if UO_2 and lithium came into contact, the specimens were clad with 80 mils of niobium-1 w/o zirconium. It was realized at the time that the cladding was thick enough to prevent study of fuel swelling. By protecting the fuel with a thick cladding, however, it was felt that observations could be made on fuel movement, microstructural changes, effect of burnup, fuel-cladding compatibility, and any possible effects of fissioning rate on the above phenomena.

EXPERIMENTAL PROGRAM

Five capsules, each containing six specimens, were irradiated. The design specimen-surface temperature was 1200 C, with fuel burnups ranging from 1.5 to 5.0 a/o of the uranium. The specimen design parameters and irradiation conditions

*References given at end.

[redacted]

TABLE 1. SPECIMEN DESIGN PARAMETERS AND DIMENSIONS FOR HIGH-TEMPERATURE UO_2 IRRADIATION

Capsule	Number of Specimens	Enrichment in U^{235}, per cent	Surface Temperature, C	Central Temperature, C	Uranium Burnup, a/o	Heat Generation, kw per cm^3	Fuel Diameter, in.	Fuel Length, in.	Void Length, in.	Cladding Thickness, in.	Specimen Diameter, in.	Specimen Length, in.
BMI-44-1	6	20	1200	2300	1.5	2.0	.225	.75	1.05	.080	.385	2.00
BMI-44-2[a]	6	20	1200	2300	3	2.0	.225	.75	1.05	.080	.385	2.00
BMI-44-3	3	16	1200	2840	3	3.0	.225	.60	1.20	.080	.385	2.00
	3	20	1200	2840	3	3.0	.225					
BMI-44-4	3	16	1200	2300	3	1.1	.290	.75	1.05	.080	.450	2.00
	3	20	1200	2300	3	1.1	.290					
BMI-44-5[a]	3	16	1200	2300	5	2.0	.225	.60	1.20	.080	.385	2.00
	3	20	1200	2300	5	2.0	.225					

(a) Target burnups of BMI-44-2 and BMI-44-5 were interchanged during the program because of thermocouple failures in BMI-44-5.

are given in Table 1. To study the effect of burnup on UO_2 performance, the specimens in Capsules BMI-44-1, -2, and -5 were of identical design, with only the length of irradiation being varied, resulting in burnups of 1.5 to 5.0 a/o uranium (3.5×10^{20} to 12×10^{20} fissions per cm^3. The specimens in Capsule BMI-44-4 were irradiated at a lower fission rate to study the effects of fission rate on fuel behavior. In order to maintain the 1200 C surface temperature and 2300 C central temperature in these specimens, it was necessary to increase the fuel diameter to 0.290 in. Specimens in BMI-44-3 were irradiated in a considerably higher flux than were the other specimens to study the effects of very high fuel center-line temperature.

After irradiation, the specimens were examined for dimensional changes and surface corrosion. The amount of fission gas released from the fuel was determined. Fuel growth was studied by gamma scanning and metallographic techniques.

COMPATIBILITY STUDIES

Prior to initiating the irradiations, a brief investigation of the compatibility of fuel-cladding-lithium at temperatures in the 1100 C range was performed. Work by other investigators had shown that lithium and niobium-1 w/o zirconium were compatible at 1200 C up to 1500 hr.[2] The rate of attack was thought to be dependent on the impurity level of the lithium and the cladding. No previous record of UO_2-lithium compatibility studies was found, and a series of brief compatibility studies was undertaken:

(1) Lithium and UO_2 at 1100 C.

(2) A compatibility test involving three defected specimens and one undefected specimen at 1200 C for 300 hr. (Radiographs were taken periodically to determine whether any attack was taking place.)

(3) Long-term compatibility tests of 3000 hr at 1200 C involving undefected UO_2 specimens clad with niobium-1 w/o zirconium in contact with lithium.

UO_2-Lithium

Two UO_2 pellets (with 96.3 per cent theoretical density and an oxygen/uranium ratio of 2.004) were immersed in lithium in a niobium-1 w/o zirconium can and heated at 1100 C. The lithium was purified by using a zirconium-titanium alloy for gettering of oxygen and hydrogen. Radiographs were taken of the specimens before heating, after 5 min at temperature, and after 90 min at temperature. These radiographs are shown in Figure 1. The first radiograph shows the sharp edges of the UO_2 pellets while some minor rounding off has taken place after 5 min of lithium attack. After 90 min of lithium attack at 1100 C, considerable crumbling of the specimens had taken

place. Three different analyses of the lithium residue showed uranium contents varying from 20 to 46 per cent.

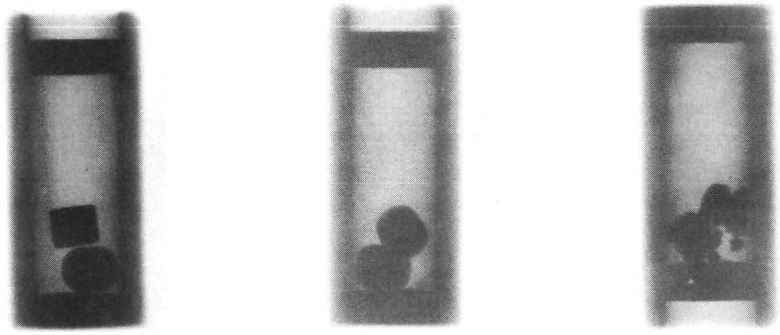

a. Before Test b. After 5 Min c. After 90 Min

FIGURE 1. RADIOGRAPHS SHOWING PROGRESSIVE LITHIUM ATTACK ON UO_2 AT 1100 C

UO_2-Lithium-Niobium-1 w/o Zirconium

This test included one undefected specimen along with three defected specimens in the same container with lithium at 1200 C. The three defected specimens had the following defects: an unfilled weld, a 40-mil hole, and a longitudinal slit the whole length of the specimen. Radiographs were taken of the specimens at various intervals (Figure 2). No attack was detected after 6 hr at 1200 C in contact with lithium. However after 150 hr, considerable attack had taken place in all but the undefected specimen. No UO_2 was left in the specimen which had a longitudinal slit in the cladding. The sample defected with the 40-mil hole had lost all of its UO_2 down to the level of the hole which was positioned at the midpoint of the cladding. The specimens with the defective weld had lost considerable amounts of UO_2. After 300 hr of testing at 1200 C in lithium, the specimens were removed from the capsule and examined visually. A photograph of the test specimens along with an untested specimen is shown in Figure 3. The niobium-1 w/o zirconium cladding underwent considerable corrosive attack.

Analysis of the lithium residue in the capsule showed that it contained considerable amounts of lithium-U_3O_8 salt. The niobium-1 w/o zirconium cladding of the specimen which had the longitudinal slit was analyzed with a microprobe analyzer. The analysis showed a uranium concentration of 60 per cent near the edge, falling off to 30 per cent at 5 mils from the edge. Uranium and niobium form solid solutions at all compositions, with the addition of uranium lowering the melting point. It seems that the reaction of lithium and UO_2 in the presence of niobium resulted in the formation of a lithium uranium oxide salt with some free uranium being taken up by the niobium-1 w/o zirconium alloy.

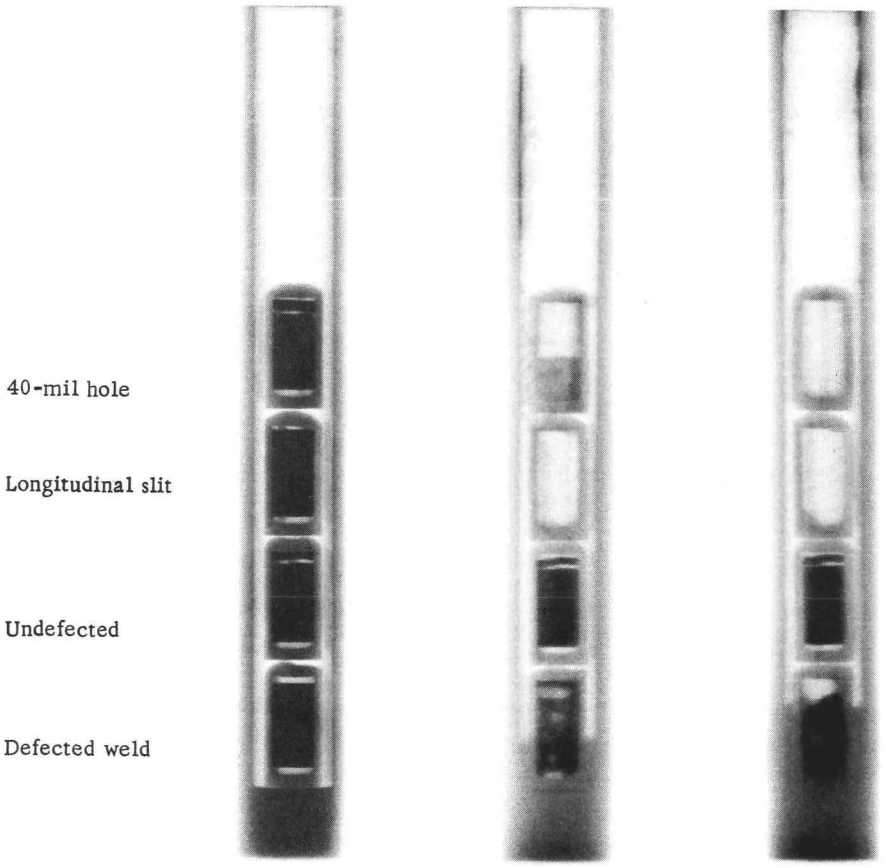

a. Before Test b. After 160 Hr c. After 300 Hr

FIGURE 2. RADIOGRAPHS OF DEFECTED SPECIMENS AFTER EXPOSURE TO LITHIUM AT 1200 C

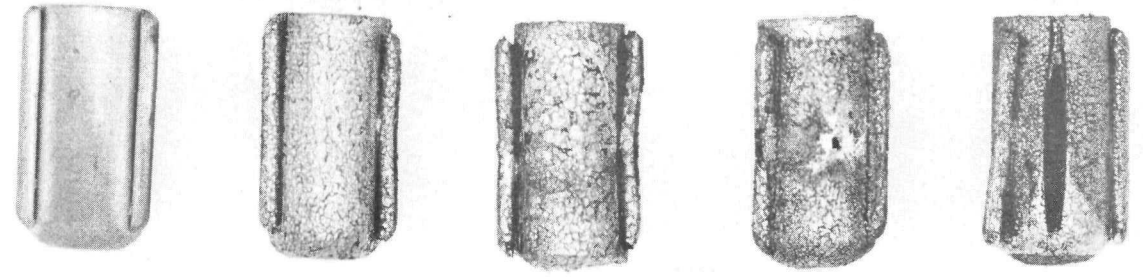

2X

RM24078

Before test | Undefected specimen | Defected weld | 40-mil hole | Longitudinal slit

FIGURE 3. COMPATIBILITY SPECIMENS AFTER EXPOSURE TO LITHIUM AT 1200 C FOR 300 HR

Lithium-Niobium-1 w/o Zirconium

Radiographs of a 3000-hr compatibility specimen (an undefected niobium-1 w/o zirconium-clad UO_2 specimen) after 300 and 1000 hr of operation at 1200 C in contact with lithium showed that no gross attack on the specimen had taken place. After 3000 hr of operation at 1200 C, the specimen was removed and examined. A continuous precipitate was found at the grain boundaries of the cladding; however, there was no direct evidence of lithium penetration in the cladding. In comparing the above specimen with the niobium-1 w/o zirconium which had been in contact with a mixture of lithium and UO_2, it was evident that the combination of lithium and UO_2 was considerably more corrosive than lithium alone. No reaction was found between the UO_2 and cladding and no changes had occurred in the UO_2 microstructure as a result of the 3000-hr heat treatment. These microstructures are shown in Figure 4.

CAPSULE DESIGN

A schematic radial cross section of the high-temperature capsule used in these irradiation experiments is shown in Figure 5. The specimens are surrounded by a 40-mil annulus of lithium contained in a 180-mil-thick niobium-1 w/o zirconium can. Thermocouples of W5Re-W20Re are located in the wall of this can. The temperature drop from these thermocouples to the specimen is about 100 C. A static helium gap is located between the niobium-1 w/o zirconium can and the first stainless steel shell. Chromel-Alumel thermocouples are located in grooves in this stainless steel shell. The temperature drop from the tungsten-tungsten-rhenium thermocouples to the Chromel-Alumel thermocouples is about 620 C when the specimen surface temperature is 1200 C.

Between the two stainless steel shells is a gas annulus containing a mixture of helium and nitrogen. The nitrogen content in the annulus is varied in order to obtain a larger temperature drop if higher specimen-surface temperatures are desired. The outer stainless steel shell is in contact with the reactor process water. Figure 6 shows the capsule components.

A more detailed description of the design and operation of this type of high-temperature irradiation capsule will appear in a forthcoming BMI report.

SPECIMEN DESIGN AND FABRICATION

In arriving at the specimen design, the most important consideration was to prevent the lithium coolant from coming into contact with the UO_2 fuel. The final specimen design utilized 80 mils of niobium-1 w/o zirconium cladding. Considerable void space was left inside the specimens in order to accommodate the expected pressure produced by fission gas released from the fuel. The design parameters for the irradiation specimens are given in Table 1, and the reasons for arriving at these parameters are discussed in Appendix A.

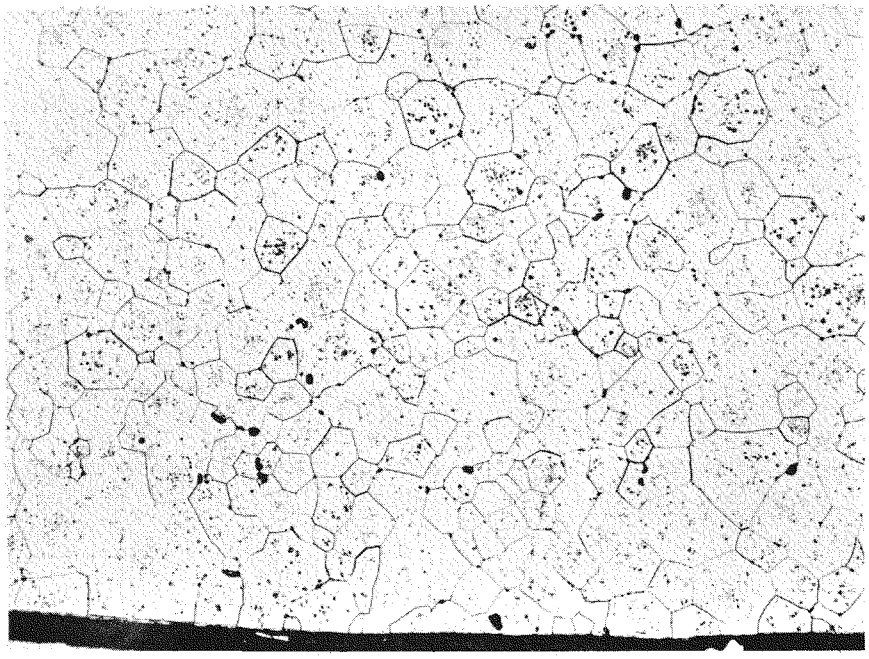

250X RM27811

a. UO_2-Niobium-1 w/o Zirconium Interface

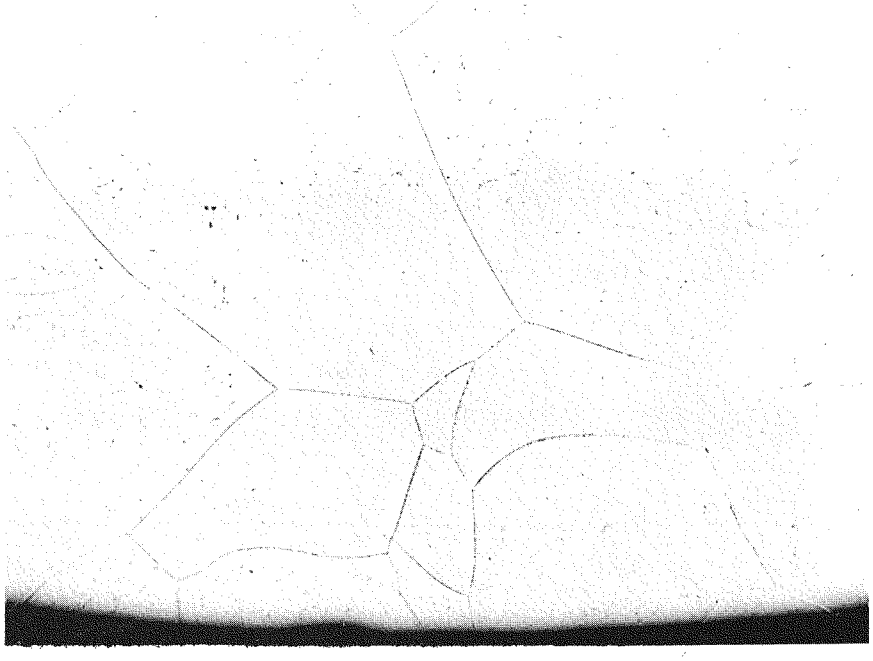

100X RM27822

b. Lithium-Niobium-1 w/o Zirconium Interface

FIGURE 4. MICROSTRUCTURE OF THE UNDEFECTED 3000-HR COMPATIBILITY SPECIMEN

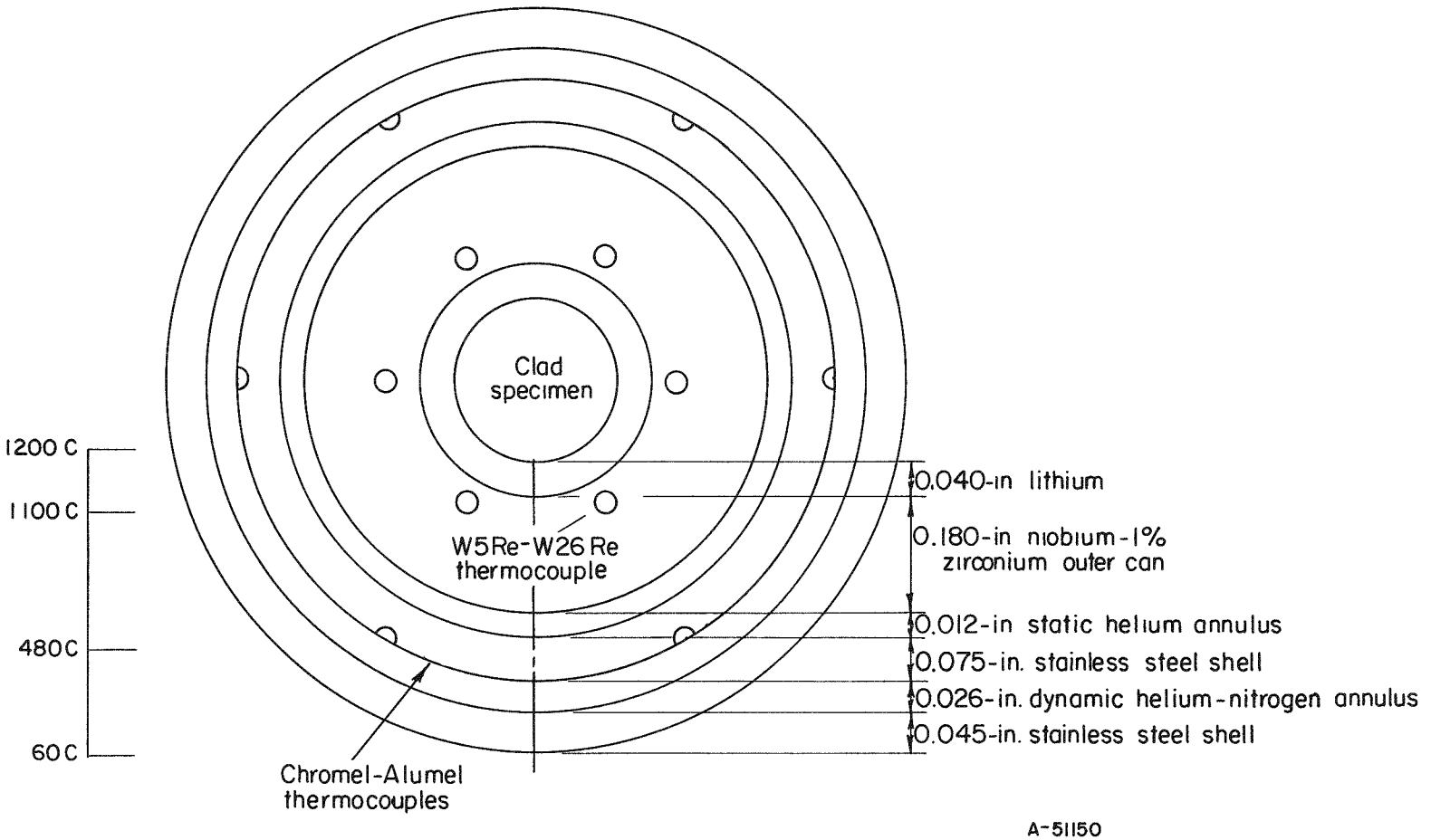

FIGURE 5. SCHEMATIC CROSS-SECTIONAL VIEW OF THE HIGH-TEMPERATURE CAPSULE

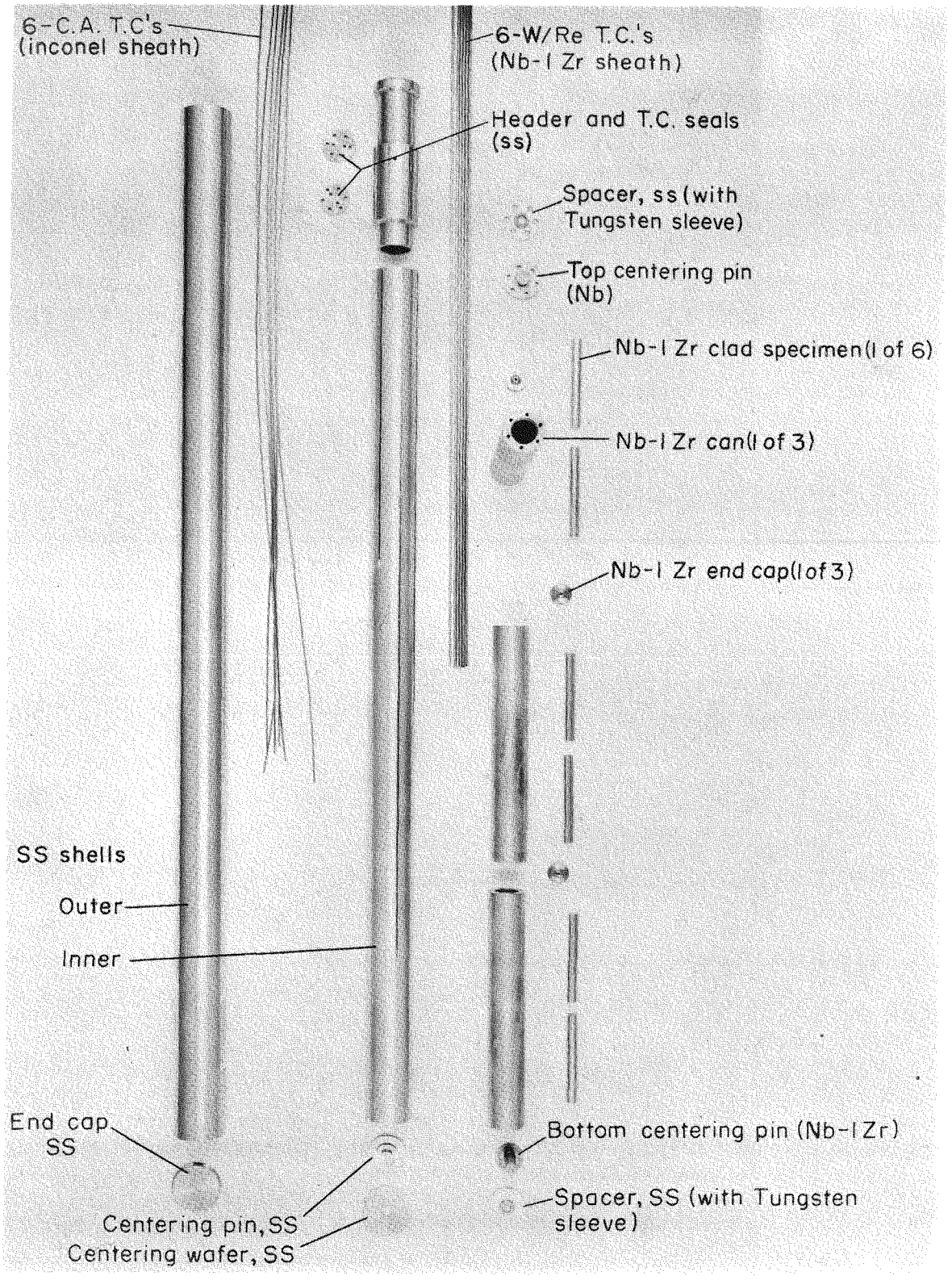

FIGURE 6. PHOTOGRAPHS OF THE HIGH-TEMPERATURE CAPSULE COMPONENTS BEFORE ASSEMBLY

Fuel Pellet Fabrication

Parametric studies indicated that a fuel of approximately 20 per cent enrichment would be necessary to provide the design heat-generation rates. Two lots of UO_2 were obtained for the fabrication of specimens. Both were a ceramic grade; however, the nominal enrichments were 16 and 20 per cent U^{235}.

Pellets for Capsule BMI-44-1 were fabricated to 94 to 96 per cent of theoretical density by prefiring the material and ball milling in 400-g batch lots with uranium slugs in a rubber-lined mill. Pellets for Capsules BMI-44-2, -3, -4, and -5 were fabricated to 95 to 96 per cent of theoretical density by milling the prefired material in a stainless steel mill. The milled materials were dried in an air atmosphere oven at 150 C, granulated, and pressed in a double-action die at 35 tsi (50 kg per mm^2). The pellets were sintered on a plate of presintered UO_2 in a flowing dry-hydrogen atmosphere for 2 hr at 1800 C. The heat-up rate was 400 C per hr with a 1-hr hold at 1300 C. The pellets were furnace cooled over a 16-hr period, with temperature drop during the first hour not exceeding 400 C. The 16 per cent enriched UO_2 was prepared in the same manner as the 20 per cent enriched UO_2. Sintered densities of 97 to 98 per cent of theoretical were measured.

Figure 7 shows typical microstructures of the 16 and 20 per cent enriched fuel pellets. The analyses of the different sintered fuel pellets are shown in Table 2.

TABLE 2. CHEMICAL ANALYSIS OF UO_2 FUEL PELLETS

Material	Contaminant Elements, ppm												
	Fe	Cr	Ni	Si	Mn	Mo	S	Sn	Cu	Ca	Al	C	O/U
16 per cent enriched pellets[a]	460	130	140	5	15	50	--	2	58	50	--	--	2.004
20 per cent enriched pellets[a]	560	160	140	15	2	15	--	T	1	5	50	--	2.005
20 per cent enriched pellets[b]	70	30	30	50	10	3	30	T	3	30	--	200	2.004

(a) UO_2 ball milled in a stainless steel mill (Capsules BMI-44-2, -3, -4, -5).
(b) UO_2 ball milled in a rubber-lined mill (Capsule BMI-44-1).

Specimen Cladding

The claddings were prepared in two sections from niobium-1 w/o zirconium rod by blind drilling the fuel cavity with an end radius. An average of five analyses on the cladding material showed the zirconium, oxygen, and hydrogen contents to be 0.85 per cent, 294 ppm, and 5.6 ppm, respectively. Natural UO_2 powder was pressed into the radius of the longer of the two sections to fill the radial void at the bottom of the specimen and thereby prevent the hot fuel from coming into contact with the cladding. The fuel pellets were slip fit into the cladding tube, followed by a 0.040-inch-thick sintered disk of natural UO_2; a tungsten spring was placed on top to maintain the UO_2 in position. A niobium-1 w/o zirconium wire was used to maintain the position of UO_2 in specimens of Capsule BMI-44-1. Figure 8 gives a schematic drawing of the specimens.

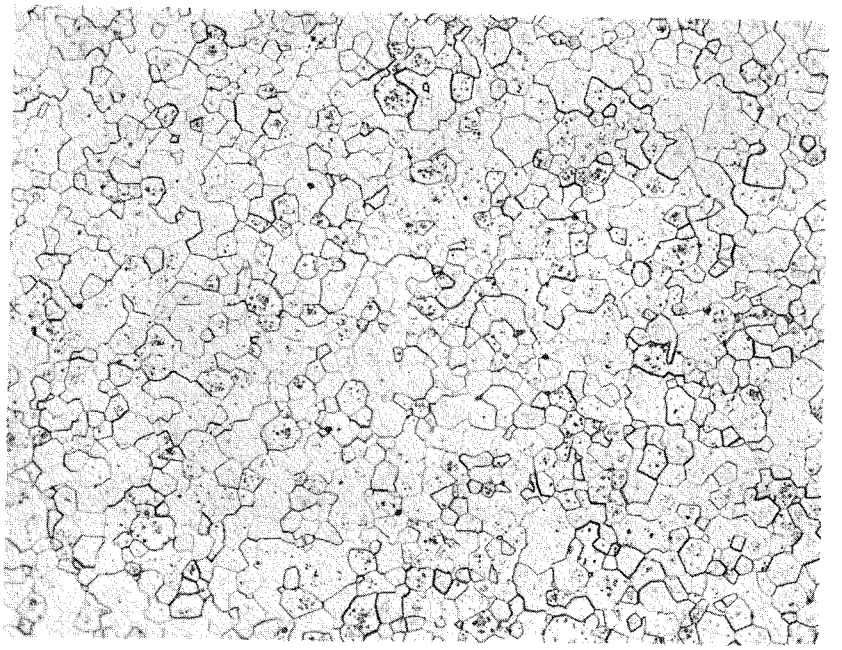

250X RM27404

a. 16 Per Cent Enriched UO_2 etched with H_2SO_4-95 Volume Per Cent H_2O_2

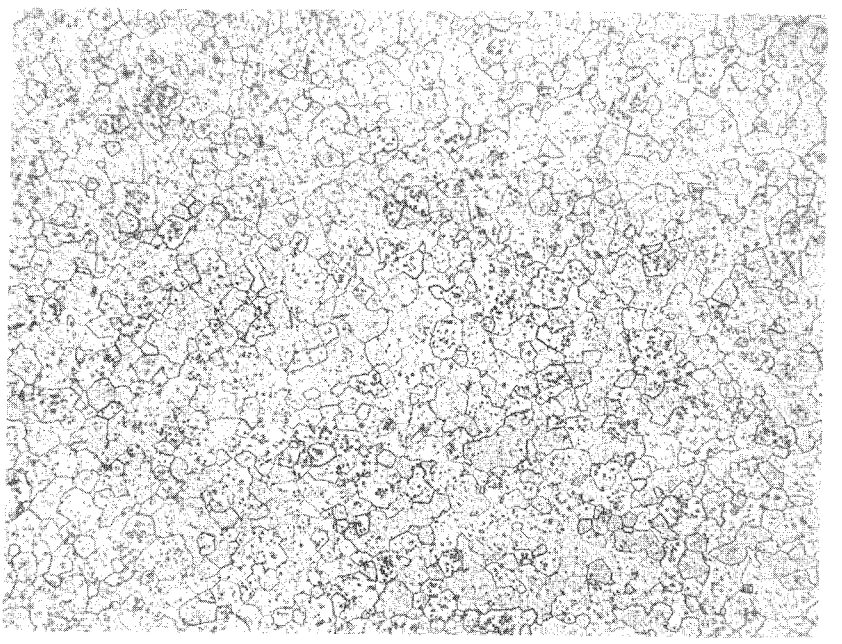

250X RM27329

b. 20 Per Cent Enriched UO_2 etched with H_2SO_4-95 Volume Per Cent H_2O_2

FIGURE 7. MICROSTRUCTURE OF UO_2 PELLETS BEFORE IRRADIATION

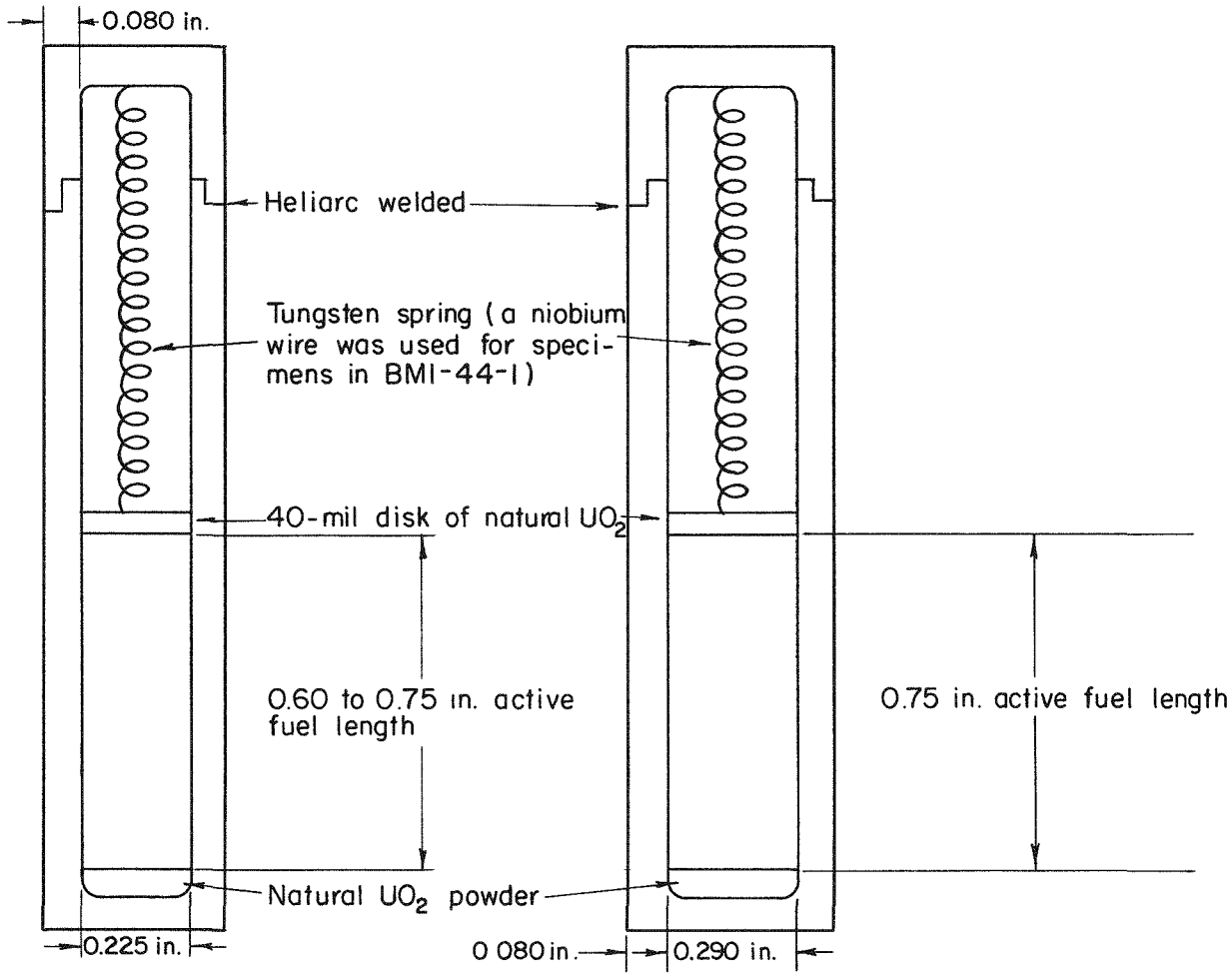

a. Specimens for capsule BMI-44-1,-2,-3 and -5

b. Specimens for capsule BMI-44-4

A-51151

FIGURE 8. SHEMATIC DRAWING OF SPECIMENS USED FOR HIGH-TEMPERATURE CAPSULES

After loading, the two cladding sections of each specimen were welded together by a tungsten arc in a helium-atmosphere dry box while maintaining an impurity level of less than 10 ppm in the helium. The excess weld metal was machined from the specimens. The specimens were then annealed in a vacuum for 1 hr at 1260 F while being monitored by a helium leak detector. The completed specimens were examined by radiography and macrographs, and dimensional measurements and densities were recorded prior to encapsulation for irradiation. Figure 9 shows a pair of welded specimens ready for encapsulation.

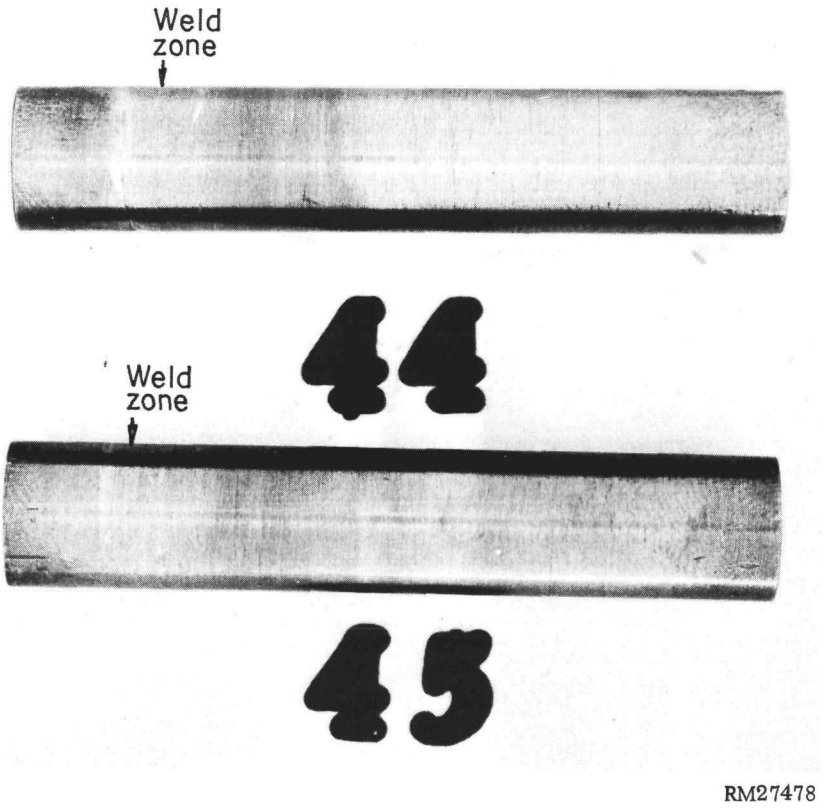

FIGURE 9. APPEARANCE OF NIOBIUM-1 W/O ZIRCONIUM CLAD UO_2 SPECIMENS BEFORE IRRADIATION

IRRADIATION HISTORY

All of the five capsules were irradiated in the Materials Testing Reactor. The estimated fuel-surface temperatures for each of the specimens in the five capsules for each cycle of irradiation as determined from thermocouple data are given in Tables 3 through 7. Temperature readings were taken every 24 hr, and both the average and the maximum temperature are given for each cycle. The following comments describe briefly the procedure used to arrive at these temperature estimates.

TABLE 3. TEMPERATURE SUMMARY FOR BMI-44-1

Cycle	Gas Mixing	Maximum Temperature of Specimen Indicated, C						Average Temperature of Specimen Indicated, C					
		1	7	2	8	4	10	1	7	2	8	4	10
196	No	315	315	760	775	1025	1220	315	315	650	760	940	1165
197-A[a]	No	400	510	815	885	1050	1220	385	440	760	815	1040	1190
197-B[a]	No	1245	1260	1345	1205	1040	900	1230	1230	1290	1165	995	870
198	No	1205	1170	1220	1135	995	845	1165	1165	1105	1065	925	760
199	No	1165	1185	1230[c]	1135	1040	980	1150	1165	1120[c]	1080	980	900

(a) Capsule was in Position A-2-SW for just 5 days of Cycle 197-A.

(b) Capsule moved to Position A-2-NE for remainder of Cycle 197-B.

(c) Chromel-Alumel thermocouple on this specimen failed. Specimen temperatures estimated on basis of readings of adjacent thermocouples and axial temperature profile for Cycle 198.

TABLE 4. TEMPERATURE SUMMARY FOR BMI-44-2

Cycle	Gas Mixing	Maximum Temperature of Specimen Indicated, C						Average Temperature of Specimen Indicated, C					
		14	20	17	19	21	22	14	20	17	19	21	22
199	Yes	1120	1165	1180	1185	1135	1135	1105	1150	1165	1180	1105	1093
200	Yes	1245	1290	1260	1275	1205	1175	1165	1220	1190	1205	1150	1120
201	Yes	1260	1300	1290	1290	1260	1245	1205	1220	1275	1275	1220	1205
202	Yes	1260	1315	1290	1315	1300	1245	1230	1300	1275	1275	1290	1190
203	Yes	1230	1260	1290	1245	1230	1220	1205	1230	1275	1230	1220	1205
204	Yes	1220	1275	1230	1230	1220	1205	1205	1260	1220	1205	1175	1150
205	Yes	1205	1290	1275	1205	1175	1150	1190	1260	1205	1150	1120	1080
206	Yes	1230	1275	1260	1260	1230	1205	1190	1260	1245	1230	1190	1150
207	Yes	1205	1275	1245	1260	1230	1190	1190	1260	1230	1230	1205	1165
208	Yes	1245	1275	1275	1245	1220	1175	1220	1260	1260	1230	1165	1120
209	Yes	1220	1260	1315	1275	1245	1220	1205	1245	1275	1230	1190	1150
210	Yes	1220	1260	1290	1230	1205	1150	1205	1245	1275	1205	1150	1095
211	Yes	1205	1260	1275	1260	1230	1190	1190	1220	1260	1190	1165	1095
212	Yes	1205	1245	1275	1230	1220	1175	1175	1220	1260	1190	1150	1120
213	Yes	1205	1260	1275	1245	1230	1190	1150	1230	1260	1205	1165	1095

TABLE 5. TEMPERATURE SUMMARY FOR BMI-44-3

Cycle	Gas Mixing	Maximum Temperature of Specimen Indicated, C						Average Temperature of Specimen Indicated, C					
		42	36	37	38	45	46	42	36	37	38	45	46
203	No	1165	1260	1260	1290	1400	1495	1040	1135	1230	1260	1345	1415
204[a]	No	1205	1300	1315	1315	1425	1395	1065	1175	1220	1230	1345	1370
205	No	1135	1220	1220	1275	1345	1385	1080	1190	1205	1260	1290	1330
206	No	1065	1165	1175	1205	1330	1400	995	1105	1140	1190	1220	1345

(a) Gas-composites mixing introduced for 11 hr.

TABLE 6. TEMPERATURE SUMMARY FOR BMI-44-1

Cycle	Gas Mixing	Maximum Temperature of Specimen Indicated, C						Average Temperature of Specimen Indicated, C					
		56	48	49	50	58	59	56	48	49	50	58	59
201	No	1315	1300	1275	1315	1290	1230	1245	1245	1245	1260	1230	1165
202	No	1260	1245	1245	1245	1275	1205	1245	1245	1245	1245	1205	1135
203	No	1260	1245	1260	1260	1245	1205	1230	1205	1245	1230	1175	1135
204	No	1205	1175	1220	1230	1220	1165	1175	1165	1215	1225	1175	1120
205	No	1230	1175	1245	1245	1245	1165	1205	1170	1220	1230	1175	1120
206	Yes	1230	1165	1260	1245	1275	1190	1175	1150	1220	1220	1220	1175
207	Yes	1205	1150	1220	1220	1230	1150	1150	1105	1205	1190	1190	1150
208	Yes	1220	1175	1205	1205	1220	1135	1190	1135	1190	1190	1190	1105
209	Yes	1205	1120	1205	1205[a]	1230	1150	1150	1095	1175	1190[a]	1205	1120
210	Yes	1245	1245	1220	1205[a]	1260	1165	1190	1165	1175	1190[a]	1205	1105
211	Yes	1220	1135	1175	1220[a]	1220	1135	1175	1120	1165	1190[a]	1205	1105
212	Yes	1190	1135	1175	1220[a]	1230	1150	1150	1120	1165	1205[a]	1205	1135
213	Yes	1220	1135	1190	1230[a]	1220	1150	1165	1105	1165	1220[a]	1190	1135

(a) Thermocouples for this specimen not operable. Specimen temperature estimated on basis of reading of adjacent thermocouples and axial temperature profile.

TABLE 7. TEMPERATURE SUMMARY FOR BMI-44-5

Cycle	Gas Mixing	Maximum Temperature of Specimen Indicated, C						Average Temperature of Specimen Indicated, C					
		30	24	25	26	34	35	30	24	25	26	34	35
200	No	970	1025	1050	1065	1050	1025	955	1010	1040	1050	1010	1010
201	Yes	1175	1220	1220	1230	1220	1190	1150	1190	1205	1220	1205	1175
202	Yes	1205	1220	1220	1245	1230	1190	1175	1205	1205	1230	1205	1175
203	Yes	1205	1230	1230	1260	1230	1205	1190	1220	1220	1250	1220	1190
204[a]	Yes	1205	1245	1245	1245	1220	1175	1190	1230	1230	1230	1205	1165
205[a]	Yes	1205	1245	1245	1245	1220	1175	1190	1230	1230	1230	1205	1165

(a) Thermocouples on Specimens 25, 26, 34 and 35 became unreliable after four days of Cycle 204. Temperatures estimated on basis of thermocouples on Specimens 30 and 24 and axial temperature profile for Cycle 203.

UNCLASSIFIED

Sheathed W5Re-W26Re thermocouples are located in axial holes in the heavy wall of the specimen containment vessel at a point within 100 C of the fuel-surface temperatures. Since these thermocouples generally become unreliable after a period of time, Chromel-Alumel backup thermocouples are incorporated in a low-temperature radial zone (480 to 700 C) to provide temperature data when the high-temperature units no longer function properly. In the event of such failure, it is necessary to extrapolate from the readings of the Chromel-Alumel thermocouples to the specimen temperatures, using as a guide the temperature readings obtained during the early portion of the irradiation. The temperature estimates included in Tables 3 through 7 were obtained by such extrapolations during the latter portions of these irradiations, inasmuch as most of the high-temperature thermocouples in the capsules became inoperable after several reactor cycles. The uncertainty level in estimating the fuel-surface temperature is about ±50 C, which represents the normal spread in the in-pile calibration curve for the W5Re-W26Re versus the Chromel-Alumel thermocouples.

To maintain specimen temperatures at the design level it was necessary in some capsules to use a flowing gas mixture of helium and nitrogen. If gas mixing was used during irradiation, it is noted in Tables 3 through 7.

The large temperature variation between the top and bottom specimens in Capsule BMI-44-3 was due to the fact that the neutron flux was considerably higher than expected for this reactor position. It was therefore necessary to irradiate the capsule near the top of the core in a region with a large variation in the flux profile.

Target burnups of Capsules BMI-44-2 and BMI-44-5 were interchanged because of thermocouple failures in Capsule BMI-44-5. Therefore Capsule BMI-44-2 was irradiated to a high burnup while Capsule BMI-44-5 was removed for examination after an estimated burnup of 3 a/o uranium.

POSTIRRADIATION EXAMINATION

The postirradiation examination of the fuel specimens was conducted at the Battelle Hot Cell Laboratory. The capsules were examined in three different groups: Capsule BMI-44-1; Capsules BMI-44-3 and BMI-44-5; and finally Capsules BMI-44-2 and BMI-44-4.

Capsule Opening

Each capsule was opened by cutting through the two stainless steel shells with a pipe cutter, after which the niobium-1 w/o zirconium compartments were removed. The tack weld connecting the compartments was broken by slightly tapping them, and each of these compartments was examined individually. The compartments appeared generally clean and shiny except for occasional darkened areas. Samples of gas from each compartment were analyzed by gamma spectrometry to determine whether any of the specimens in the compartments had failed and thereby released their fission gases. No fission gases were found in any of the 15 compartments that were sampled for

fission gases. This substantiated the later findings that no cladding failures took place in any of the 30 specimens.

The top of each compartment was removed by a pipe cutter and the contained lithium was reacted. The lithium in the compartments from Capsule BMI-44-1 was reacted with Cellosolve. However, this proved to be a slow process and the lithium in the compartments of the other capsules was reacted with water. Before using water as a reactant, tests were performed on unirradiated specimens and the tests showed no apparent detrimental effects on the niobium-1 w/o zirconium cladding. After all the lithium had been reached, the specimens were removed from the compartments.

The residue of the lithium-water reaction from the bottom compartment of Capsule BMI-44-3 was analyzed for fission products. This compartment was chosen because it contained specimens which had been at the highest operating temperatures. Analysis of the residue revealed that 0.23 per cent of the Cs^{137} produced in the fuel had diffused through the cladding. Zr^{95}, Ru^{103}, Nd^{147}, Ce^{141}, and Ba^{140} were found to be present in quantities of about 10^{-5} per cent of that produced in the fuel.

After removal from the compartments, each specimen was visually examined. The appearance of most of the specimens was generally similar to the preirradiation appearance, with most of them being shiny and some having been darkened somewhat. Two of the specimens had undergone some local attack at the surface (Figure 10). These attacks can probably be attributed to some contamination on the specimen surface which reduced corrosion resistance to lithium at 1200 C in that area. Typical uncorroded irradiated specimens are shown in Figure 11.

Dimensional Measurements

Dimensional measurements were made on all of the 30 specimens with a micrometer. These measurements showed that the specimens underwent no dimensional changes as a result of irradiation.

Gamma Scanning

After the dimensions of the specimens were measured, all of the specimens were gamma scanned. The purpose of the gamma scanning was to compare the relative burnup of the fuel in the specimens and to measure any axial fuel growth.

The gamma scanning was accomplished by moving the specimens lengthwise and vertically past a slit in front of the window of a sodium iodide scintillation crystal. The pulses from the crystal were recorded with a pulse-height analyzer. Energy scans of the specimens showed prominent peaks at energies of 0.53 and 0.74 Mev. These energies correspond to Ru^{103} and Zr^{95}-Nb^{95} peaks, respectively. The Zr^{95}-Nb^{95} peak was selected for scanning the activity along the length of the specimens.

The gamma scans showed that considerable movement of the fuel had taken place in the axial direction as a result of irradiation. The amount of fuel movement is shown

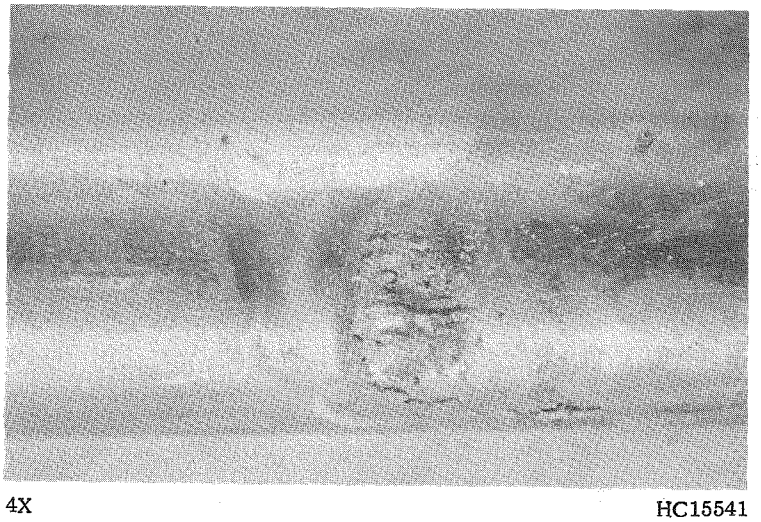

4X HC15541

a. Specimen 19 from Capsule BMI-44-2

6X HC14460

b. Specimen 30 from Capsule BMI-44-5

FIGURE 10. PHOTOGRAPHS SHOWING CORRODED AREAS ON TWO OF THE IRRADIATED SPECIMENS

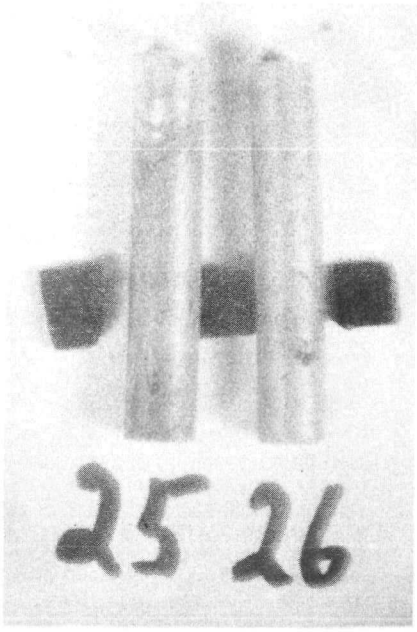

1X HC14452

a. Specimens 25 and 26 from Capsule BMI-44-5

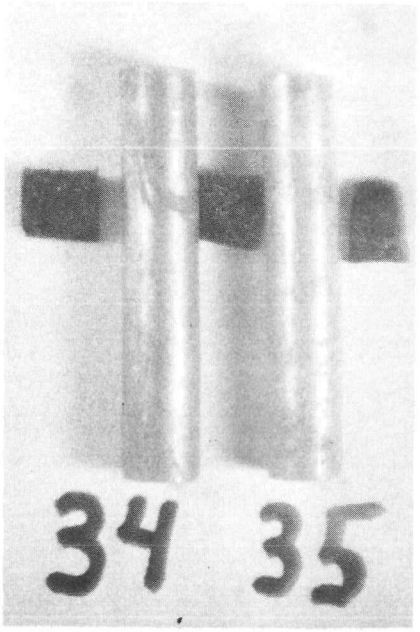

1X HC14455

b. Specimens 34 and 35 from Capsule BMI-44-5

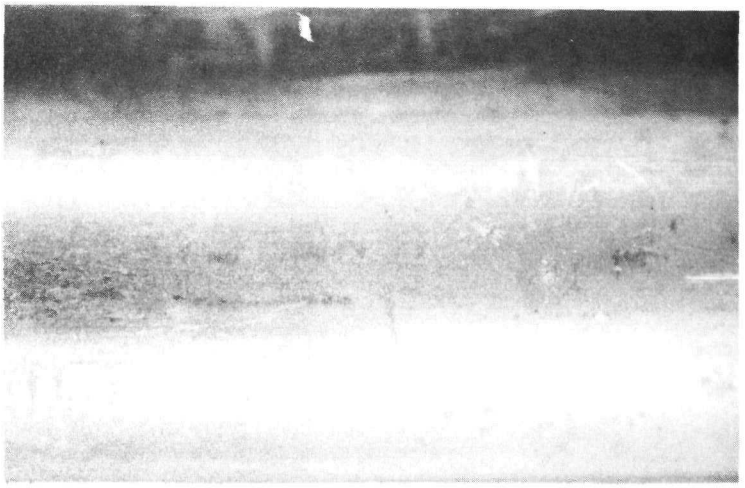

4X HC15543

c. Specimen 48 from Capsule BMI-44-4

FIGURE 11. TYPICAL IRRADIATED SPECIMENS WHICH DO NOT SHOW ANY ATTACK AS A RESULT OF IRRADIATION

The apparant bowing is due to optical distortion.

in Table 8. The reasons for and mechanism of the fuel movement will be discussed in a later section. It was not possible to use the gamma scans for relative burnup measurements because later studies showed that the central voids were not uniform and therefore the relative magnitudes of emitted gamma radiation did not represent relative burnups, but rather the relative amounts of fuel present at a particular cross section.

Burnup Determinations

Analysis of the fuel for burnup was attempted by mass spectrometry and radiochemical determinations based on Cs^{137} and Ce^{144}. The radiochemical analyses exhibited wide scatter and inconsistencies, perhaps attributable to cesium and cerium movement in the fuel, and therefore the data are not reported. For the burnup sample, a complete cross section of the specimen varying from 0.1 to 0.3 inch in length was used. Sections from three different specimens in each capsule were analyzed.

For the isotopic analyses, the relative percentages of uranium isotopes in the samples were determined by mass spectrometry. This was done for both the irradiated samples and an unirradiated control sample. The burnups were then determined from the changes in the isotopic concentrations. Difficulty was encountered in determining the isotopic composition of unirradiated controls because the enrichment of the UO_2 fuel appeared to be nonhomogeneous. The U^{235} content of the unirradiated control specimens was found to be 18.1, 18.1, 18.5, and 19.5 per cent by four different analyses at Battelle. Three analyses performed at the Chemical Processing Plant, NRTS, in Idaho resulted in values of 18.75, 19.29, and 19.43 per cent, while the UO_2 vendor quoted an enrichment of 19.91 per cent.

Three different equations were used to calculate the fuel burnup, with different assumptions being made for each of the equations:

(1) Negligible U^{238} change; independent of capture to fission-cross-section ratio for U^{235}.

(2) Capture to fission-cross-section ratio of U^{235} is 0.185, independent of U^{238}.

(3) Capture to fission-cross-section ratio of U^{235} is 0.185; negligible U^{238} change.

The equations used for the burnup calculations are given in Appendix B. Equations (1) and (2) resulted in large ranges of burnup, with Equation (2) giving consistent results. This was expected since Equation (2) is dependent on the amount of U^{236} produced and is insensitive to original U^{238} content, while Equations (1) and (3) are very much dependent on original enrichment. Thus, Equation (2) is insensitive to inhomogeneities in enrichment, and gives what are believed to be the most reliable burnup results.

TABLE 8. FUEL MOVEMENT INSIDE UO_2 SPECIMENS

Capsule	Specimen	Increase in Fuel Length[a], per cent	Central Void[b], per cent of diameter	Maximum Surface Temperature, C	Final Heat Generation, w per cm	Bulk Heat Generation of Fuel, kw per cm	Estimated Maximum Central Temperature at Start, C	Estimated Maximum Temperature of UO_2 After Fuel Movement, C
BMI-44-1	1	47	--	1245	350	2.07	2340	--
	7	55	40	1260	383	2.34	2495	2030
	2	75	50	1345	365	2.56	2700	1965
	8	55	40	1205	398	2.44	2490	1965
	4	31	25	1050	414	2.19	2200	1900
	10	28	41	1220	435	2.20	2370	2040
BMI-44-5	30	15	35	1205	378	1.51	2090	1960
	24	13	40	1245	380	1.45	2145	1970
	25	22	32	1245	350	1.44	2140	1955
	26	33	--	1260	317	1.42	2205	--
	34	26	34	1230	320	1.41	2135	1875
	35	26	33	1205	320	1.41	2110	1860
BMI-44-2	14	27	40	1260	410	2.02	2325	2045
	20	23	44	1315	415	2.02	2385	2075
	17	20	38	1315	420	2.02	2385	2090
	19	36	38	1315	380	2.03	2385	2030
	21	28	36	1300	405	2.07	2385	2100
	22	29	--	1245	385	1.97	2285	--
BMI-44-3	42	85	60	1205	372	2.38	2645	1745
	36	83	50	1300	418	2.60	2900	2010
	37	100	57	1315	403	2.74	3000	1935
	38	84	--	1315	475	2.94	3145	--
	45	145	65	1425	430	3.63	3545	1990
	46	110	50	1495	527	3.82	3775	2395
BMI-44-4	56	44	34	1315	374	1.24	2445	2070
	48	40	36	1315	392	1.22	2465	2090
	49	40	36	1300	400	1.24	2470	2090
	50	46	40	1275	373	1.22	2415	1985
	58	44	34	1290	389	1.26	2460	2070
	59	18	--	1230	453	1.24	2360	--

(a) Accuracy of measurement varies from 7 to 15 per cent, depending on the percentage of growth. The more growth in the specimen the more accurate the measurement.

(b) Considerable variation was present in the void diameter; the number given is the diameter which was the most representative.

Another set of burnup values was determined by calculating the heat flow from the specimens. This was accomplished by using the thermal conductivities of the capsule materials and the temperatures obtained from the W5Re-W26Re thermocouples, the Chromel-Alumel thermocouples, and the reactor-cooling-water temperature. These burnup results are given in Table 9.

Another method of determining burnup is the conversion of high-cross-section Xe^{135} to Xe^{136} during irradiation. Other investigators have derived a curve for the conversion of Xe^{135} to Xe^{136} as a function of effective thermal flux.[3] By using data from the mass spectrometric analyses of the fission gases in the specimens, the effective flux and, consequently, the burnup was calculated.

In comparing all the methods of burnup determination, it is believed that the ones based on mass spectrometry utilizing Equation (2) are the most accurate. Burnup based on Xe^{135} conversion is not considered accurate because most of the Xe^{135} is in the void at the top of the specimen and the neutron flux causing conversion is not attenuated as the neutron flux is in the fuel. Therefore the burnup would be somewhat high as is apparent in the data in Table 9. The burnup data based on temperature measurements are in rather good agreement with the mass spectrometry data.

Fission-Gas Release

A hole was drilled in the specimen cladding and the contained gases were collected in a system of known volume. From this system, small calibrated vials containing the fission gases were sealed and removed for analysis of Kr^{85} by gamma spectrometry. The results of the fission-gas analysis are given in Table 10.

Other investigators have reported that 100 per cent fission-gas release occurs if UO_2 temperatures exceed 1600 C.[4] By using the maximum surface temperature and the average heat-generation rate corrected for fuel growth, calculations were made to determine the percentage of fuel which was above 1600 C in these experiments. The results of such calculations and the associated gas-release data are given in Table 10. Good qualitative agreement was obtained for most specimens, although the calculation of fuel volume above 1600 C was subject to at least two sources of error:

(1) The size of the central void varied considerably from one end of the specimen to the other. This was caused by the expected axial flux variation and consequent vaporization-redeposition. It was thus difficult to select the best diameter for the central void in specimens which were sectioned transversely in just one location.

(2) The second source of error is the variation of specimen surface temperatures during irradiation. If the maximum temperatures occurred toward the end of the irradiation, the volume of UO_2 above 1600 C would be increased and the gases produced in the earlier part of the irradiation would be released. However, if the maximum temperatures occurred in the early part of the irradiation and subsequently decreased to below 1600 C, very little further fission-gas release would take place from that UO_2.

TABLE 9. BURNUP OF UO_2 SPECIMENS

Capsule	Specimen	Burnup, a/o of uranium fissioned			Burnup[a], 10^{20} fissions per cm^3 of fuel
		Isotopic[a]	Xe^{135} Conversion[b]	Heat Balance[c]	
BMI-44-1	1	1.4	1.6, 2.0	1.0	3.3
	7	--	1.3, 1.4	1.2	--
	2	1.8	1.2, 2.2	1.3	4.2
	8	--	1.2, 1.5	1.3	--
	4	--	1.4, 1.5	1.3	--
	10	1.5	1.6, 1.7	1.2	3.5
BMI-44-5	30	2.4	2.2, 2.8	2.1	5.6
	24	--	2.2, 3.0	2.1	--
	25	2.3	2.5, 2.8	2.2	5.4
	26	--	2.5, 3.1	2.3	--
	34	2.3	2.5, 3.7	2.3	5.4
	35	--	2.1, 2.2	2.3	--
BMI-44-2	14	6.0	6.7, 7.0	5.8	14.1
	20	--	5.2, 5.9	5.8	--
	17	5.9	5.2, 5.9	5.8	13.8
	19	--	5.4, 5.9	5.8	--
	21	6.0	6.1, 7.1	5.7	14.1
	22	--	6.2, 6.7	5.6	--
BMI-44-3	42	2.4	2.6, 2.6	2.1	5.6
	36	--	1.9	2.3	--
	37	2.7	2.6, 2.9	2.4	6.3
	38	--	2.5, 2.9	2.5	--
	45	3.6	3.0, 3.1	2.6	8.4
	46	--	3.2	2.7	--
BMI-44-4	56	3.1	3.2, 3.8	3.0	7.2
	48	--	3.4, 3.5	2.9	--
	49	3.3	4.0, 4.0	3.1	7.7
	50	--	3.4, 4.0	3.1	--
	58	3.2	2.9, 3.2	3.0	7.4
	59	--	2.6, 2.6	2.8	--

(a) Based on mass-spectrometry data; assumptions are that capture-to-fission cross-section ratio of U^{235} is 0.185; independent of U^{238}.

(b) Based on conversion of Xe^{135} to Xe^{136}, two mass spectrometric analyses were available from most specimens.

(c) Based on thermocouple measurements in capsule giving heat generation from which burnup was calculated.

[redacted] UNCLASSIFIED

TABLE 10. FISSION-GAS RELEASE FROM UO_2 SPECIMENS

Capsule	Specimen	Surface Temperature, C		Percentage of Fuel Above 1600 C[a] After Axial Growth	Fission-Gas Release, per cent
		Average	Maximum		
BMI-44-1	1	1150	1245	--	56
	7	1165	1260	54	51
	2	1120	1345	59	57
	8	1080	1205	47	49
	4	980	1050	37	35
	10	900	1220	28[b]	32
BMI-44-5	30	1180	1205	48	77
	24	1215	1245	51	66
	25	1230	1245	50	70
	26	1235	1260	--	80
	34	1210	1230	37	80
	35	1175	1205	33	72
BMI-44-2	14	1195	1260	57	70
	20	1245	1315	55	69
	17	1245	1315	60	66
	19	1215	1315	51	65
	21	1190	1300	62	63
	22	1140	1245	--	61
BMI-44-3	42	1045	1205	29	76
	36	1150	1300	58	87
	37	1210	1315	54	77
	38	1240	1315	--	69
	45	1300	1425	55[c]	79
	46	1365	1495	79[d]	78
BMI-44-4	56	1190	1315	62	65
	48	1160	1315	63	62
	49	1200	1300	62	57
	50	1210	1275	55	62
	58	1205	1290	60	63
	59	1135	1230	--	52

(a) Based on the maximum surface temperature.
(b) Based on a maximum temperature of 1000 C because the 1220 C occurred in the first cycle.
(c) Based on 1345 C because the 1425 C occurred in early part of the irradiation.
(d) Based on 1400 C because the 1495 C occurred in early part of the irradiation.

Metallographic Examination

Ten transverse and 20 longitudinal sections from the 30 irradiated specimens were examined metallographically. These sections were cut from locations chosen so that the microstructure caused by all possible operating conditions could be observed. In general, the pertinent macroscopic observations made concerning the fuel were as follows:

(1) A central void was formed in all of the specimens examined. The size of the central void varied considerably (Figure 12) with a larger void being formed in specimens which had operated at the highest surface temperatures at the highest fissioning rates. It can also be seen in Figures 13, 14, and 15 that the diameter of the central void varied at different places along the specimen axis. The estimated size of the central void in the various specimens is given in Table 8.

(2) The movement of the fuel in the axial direction appears to be a vaporization-deposition mechanism. This is based on the fact that the tungsten spring, which was placed on top of the fuel to keep it in place, was surrounded by UO_2 as is shown in Figures 14, 15, and 16. If the fuel movement had been due to swelling in the axial direction, the spring would have been compressed instead of being surrounded by the fuel. The bridging at the end of the fuel shown by some of the specimens from Capsule BMI-44-1 (Figure 13) may be due to the different construction of those specimens. As noted earlier, specimens in Capsule BMI-44-1 did not have a tungsten spring to keep the fuel in place. Instead, a crimped piece of niobium wire was used. Preirradiation radiographs of the specimens showed that the wire was ineffective in keeping the thin plate of natural UO_2 in place in some of the specimens. It is, therefore, quite likely that the plate of natural UO_2 was free to move about. In specimens in the other capsules, the spring kept the platelet in contact with the fuel and consequently the center of the platelet became hot enough to vaporize and deposit around the spring in the top part of the specimen.

Figures 17 and 18 show that there is a definite relationship between maximum hypothetical central temperature and fuel growth and void formation. The maximum hypothetical central temperature is directly dependent on fissioning rate, with a higher temperature resulting from a high fissioning rate. Table 8 lists the calculated maximum central temperatures (based on linear heat generation in the pellet before the fuel movement took place) and maximum surface temperature. Some of the quoted temperatures are unreasonably high since they exceed the melting temperature of UO_2, but the number serves as a measure of the relative severity of the thermal conditions inside the UO_2.

Table 8 also lists the calculated temperature of the UO_2 at the surface of the central void. This temperature is based on the maximum specimen exterior surface

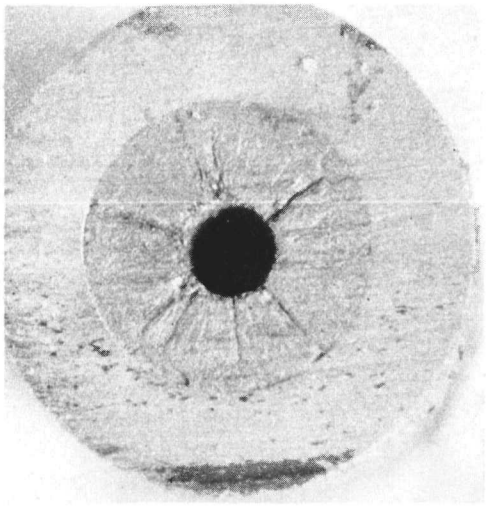

6X HC15314

a. Specimen 24 from Capsule BMI-44-5

Maximum surface temperature was 1245 C; bulk heat generation was 1.4 kw per cm^3.

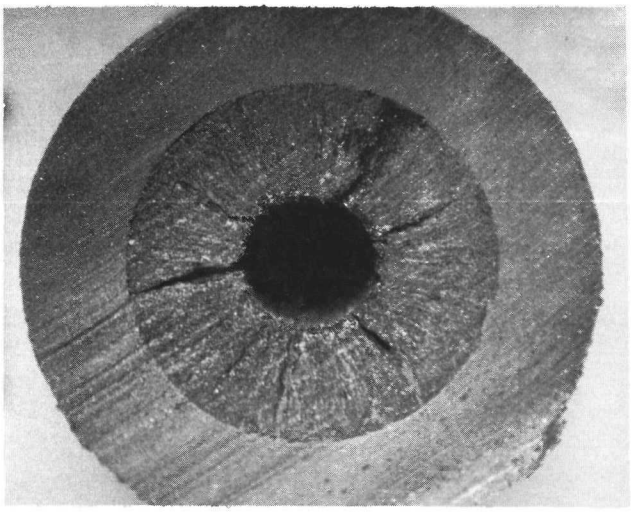

6X HC15711

b. Specimen 49 from Capsule BMI-44-4

Maximum surface temperature was 1300 C; bulk heat generation was 1.3 kw per cm^3.

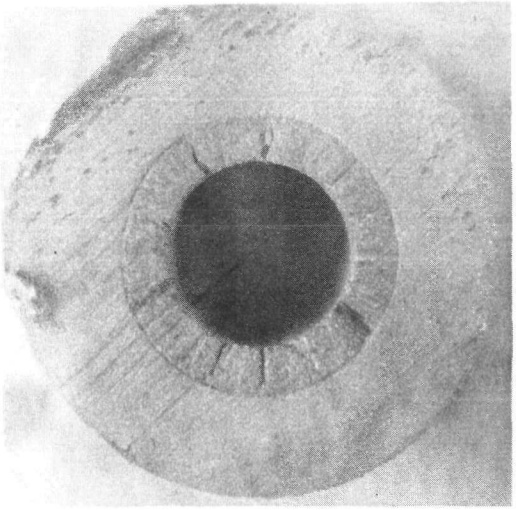

6X HC15331

c. Specimen 45 from Capsule BMI-44-3

Maximum surface temperature was 1425 C; bulk heat generation was 3.6 kw per cm^3.

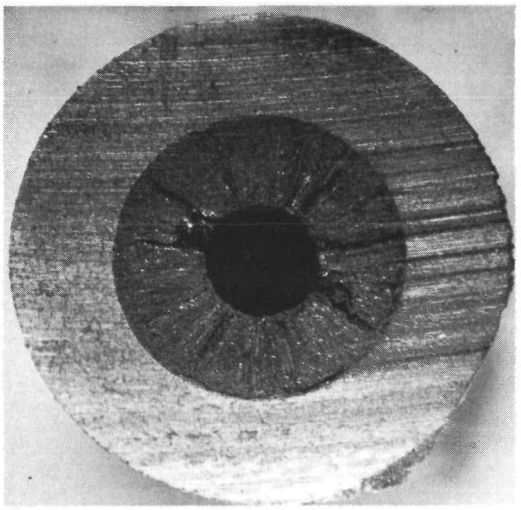

6X HC15698

b. Speimen 17 from Capsule BMI-44-2

Maximum surface temperature was 1315 C; bulk heat generation was 2.0 kw per cm^3.

FIGURE 12. TRANSVERSE SECTIONS OF VARIOUS SPECIMENS SHOWING THE CENTRAL VOID SIZE AT VARIOUS TEMPERATURES AND HEAT RATINGS

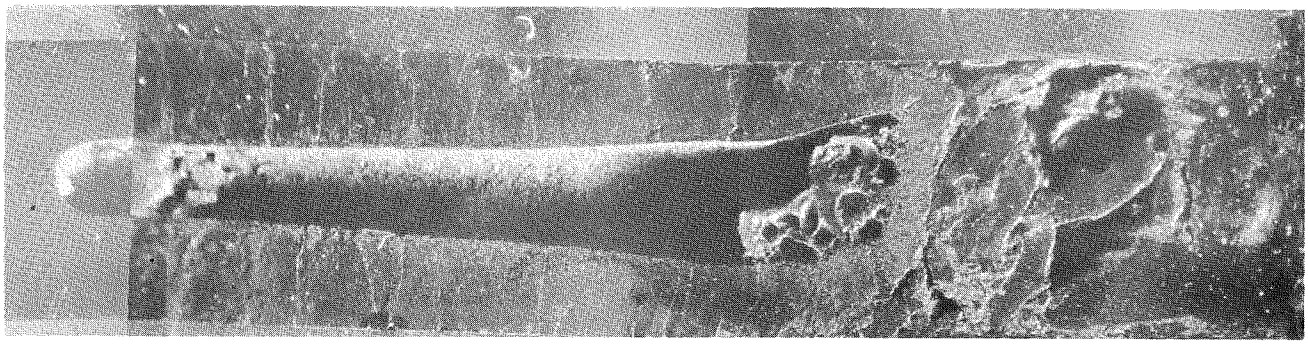

4X HC13833, HC13834 & HC13835

a. Specimen 4

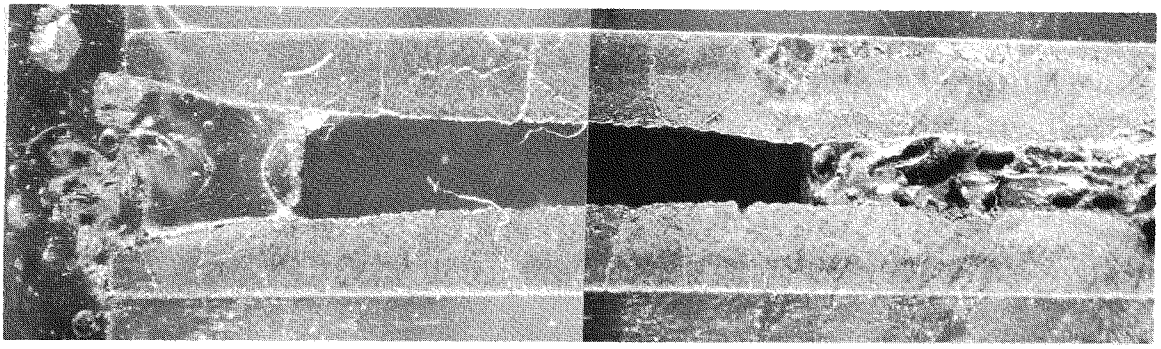

4X HC13839 & HC13841

b. Specimen 7

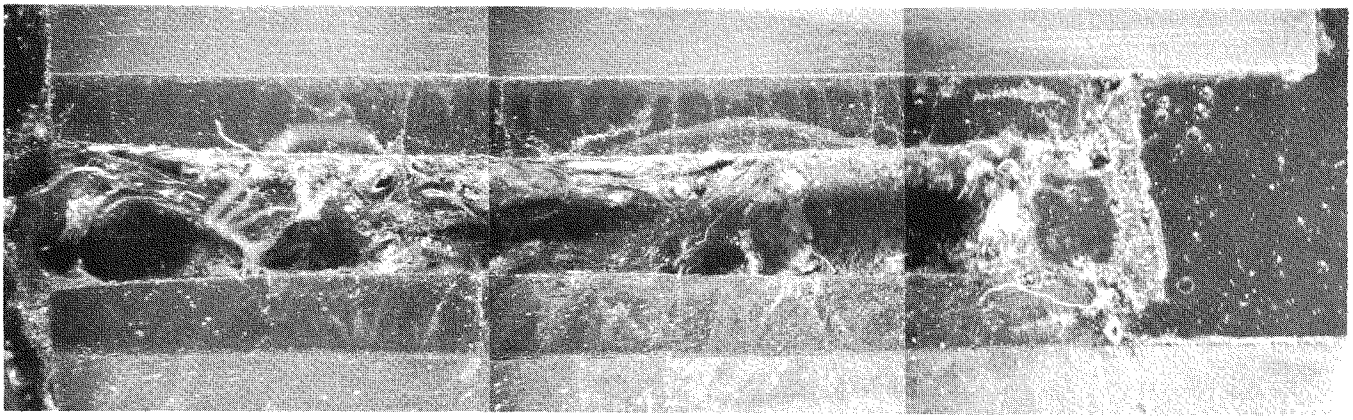

4X HC13835, HC13836 & HC13837

c. Specimen 8

FIGURE 13. LONGITUDINAL SECTIONS OF SPECIMENS FROM CAPSULE BMI-44-1

Note the uneveness of the central voids and end "cap" at the end of the fuel in Specimen 4.

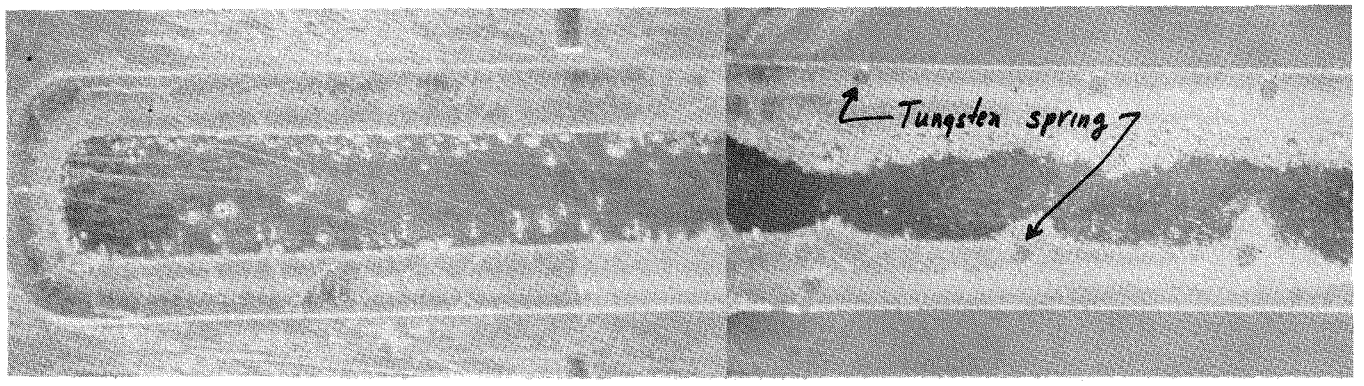

6X HC15488 and HC15491

a. Specimen 46

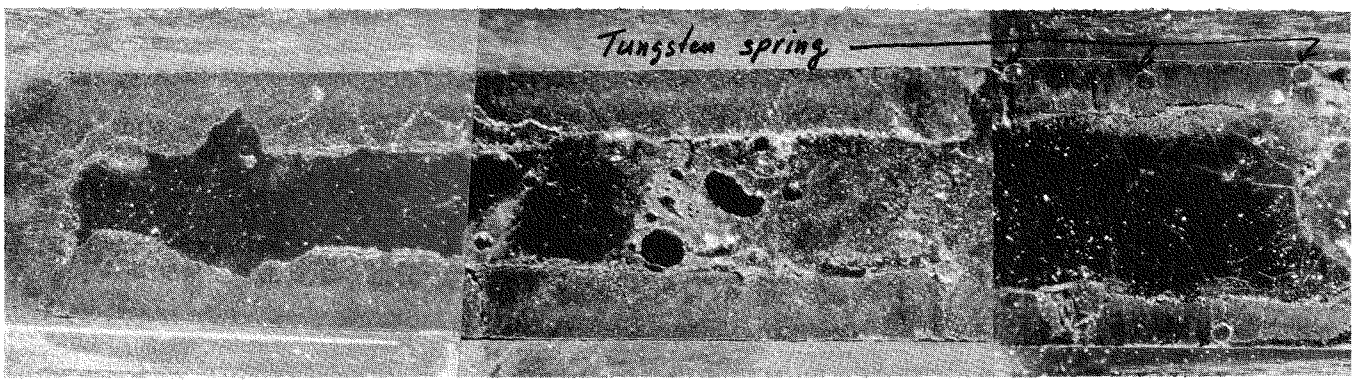

6X HC14845, HC14847 and HC14849

b. Specimen 36

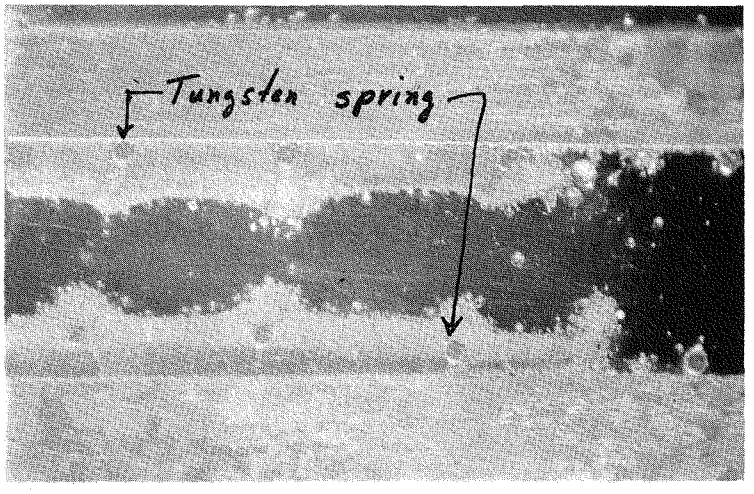

6X HC15496

c. Specimen 45

FIGURE 14. LONGITUDINAL SECTIONS OF SPECIMENS FROM CAPSULE BMI-44-3

Note the UO_2 surrounding the tungsten spring.

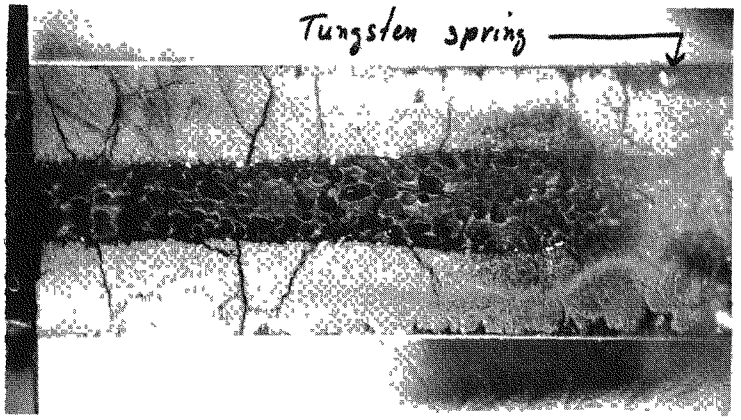

6X HC16702

a. Specimen 14 from Capsule BMI-44-2

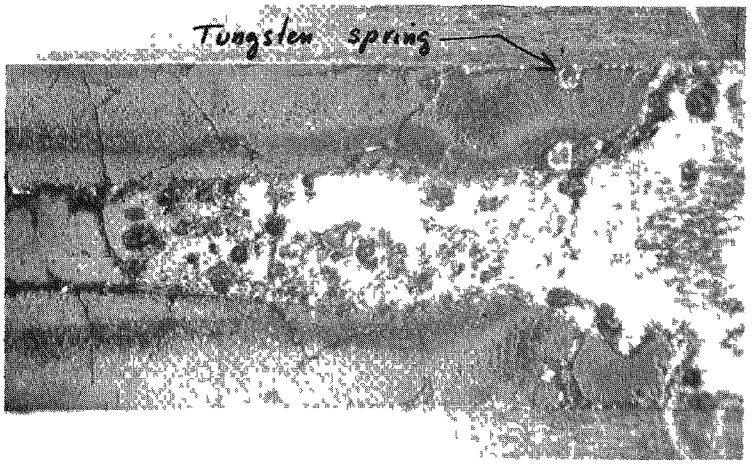

6X HC16708

b. Specimen 49 from Capsule BMI-44-4

FIGURE 15. LONGITUDINAL SECTIONS OF SPECIMENS FROM CAPSULES BMI-44-2 AND BMI-44-4

Note the UO_2 surrounding the tungsten spring.

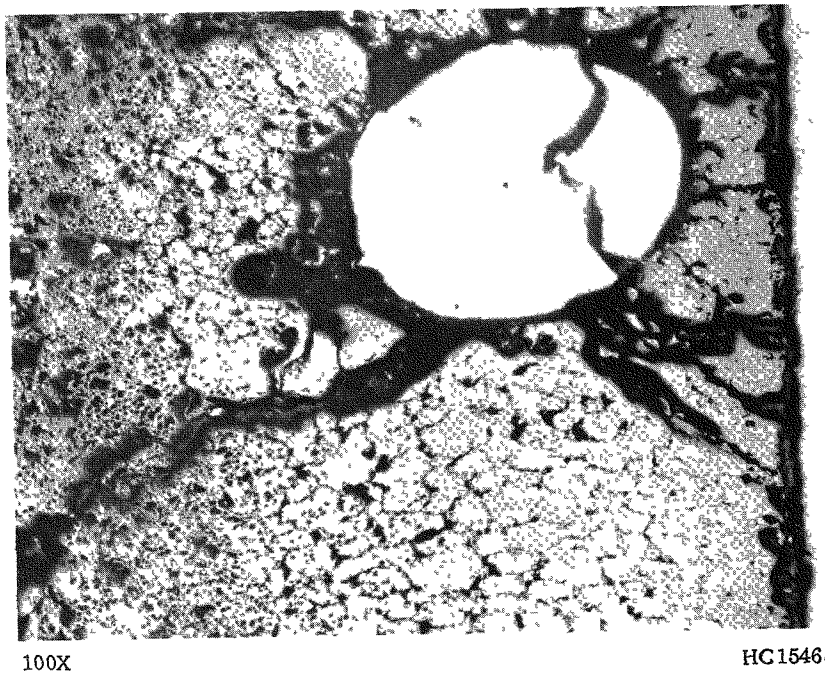

100X HC15465

a. Specimen 46 from Capsule BMI-44-3

(As-Polished)

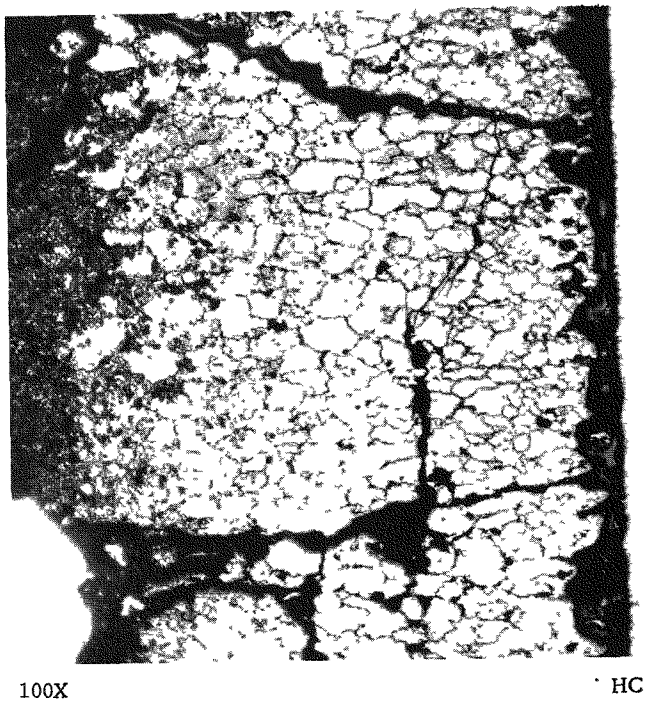

100X HC15404

b. Specimen 45 from Capsule BMI-44-3

(Etched)

FIGURE 16. MICROSTRUCTURE OF THE VAPOR-DEPOSITED UO_2 SURROUNDING THE TUNGSTEN SPRING

Also note the white particles which are believed to be either tungsten or niobium rather than free uranium.

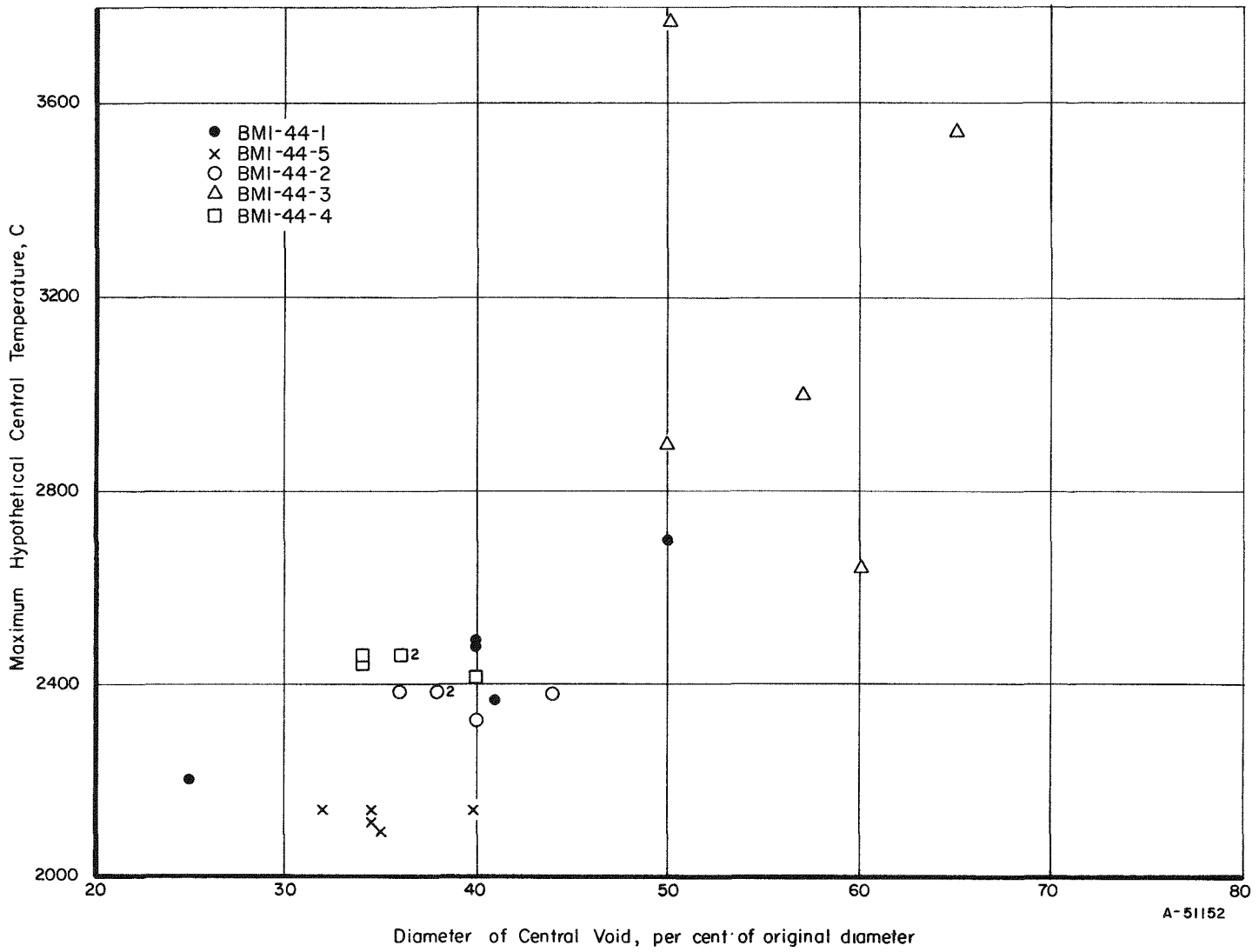

FIGURE 17. CENTRAL-VOID FORMATION AS A FUNCTION OF MAXIMUM HYPOTHETICAL CENTRAL TEMPERATURE

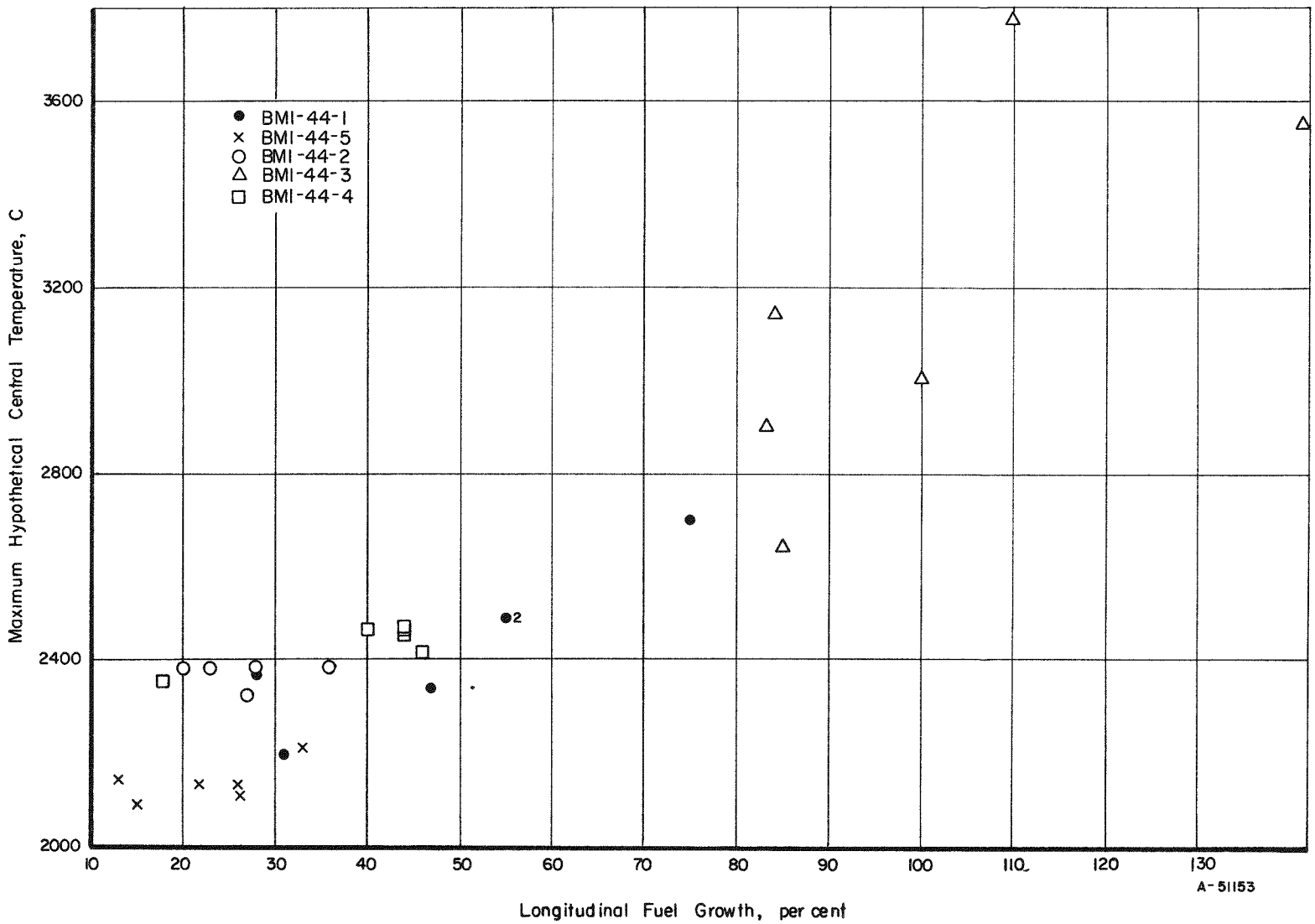

FIGURE 18. FUEL GROWTH AS A FUNCTION OF MAXIMUM HYPOTHETICAL CENTRAL TEMPERATURE

temperature, size of central void, and the final linear heat-generation rate, allowing for final fuel configuration. Most of the data indicate final maximum specimen temperatures of 1900 to 2100 C. At these temperatures UO_2 has a significant vapor pressure. This indicates that UO_2 will vaporize and then redeposit until the maximum temperature is reduced to about 1900 to 2100 C. The variation in the temperature is due to the uncertainty of void diameters, as discussed in the section on fission gases. The fuel movement appears to take place rapidly, since no dependence on burnup is evident in Figures 17 and 18. Also, in no case was all of the available void volume taken up by the movement of UO_2. Therefore it seems that the final equilibrium configuration is dictated by the thermal conditions inside the specimen. After the establishment of the stable configuration in the early part of irradiation, the fuel behaves as if it had been a hollow element originally.

Microscopic examination of the specimens revealed the following:

(1) The general microstructure of the specimens consisted of as-sintered small equiaxed grains near the outer edge of the fuel, with the grains becoming larger and more elongated further away from the edge. The grains finally become columnar, and toward the center of the fuel, the grains again become equiaxed, although they are considerably larger than the grains at the outside edge. This microstructure is illustrated in Figures 19, 20, and 21.

(2) The microstructure, as it is described above, is the same for the fuel at all locations along the longitudinal axis. This holds true for the "original" fuel as well as for the fuel which was "redeposited". Figures 22 and 23 show both the "original" and "redeposited" microstructures.

(3) There were few large fission-gas bubbles in the fuel as shown in Figures 19, 20, and 21. The few gas bubbles which were present appeared to be rather small. The lack of large fission-gas bubbles could be the result of the relatively high rate of fission-gas release from the fuel.

(4) The presence of small white particles was noted in the fuel (Figures 16, 23, and 24). It was not possible to definitely identify these particles, although they appeared similar to material identified as either free uranium or refractory metals by other investigators.[5,6,7] These particles did not etch with H_2SO_4. This would indicate that the particles were not uranium; however, work at other sites has shown that free uranium becomes resistant to acids after long irradiation times. This is supposedly caused by the alloying effect of fission products.

Investigators who have claimed that the white particles are free uranium have attributed these particles to precipitation of uranium on cooling if the UO_2 is heated above 1800 C, forming UO_2 and uranium at lower temperatures. They have found the white particles to be present in those regions of the UO_2 which have been at temperatures above 1800 C; namely, in the columnar grains. However, in these specimens some white particles were found near the surface of the UO_2, a region which presumably had not been above 1800 C.

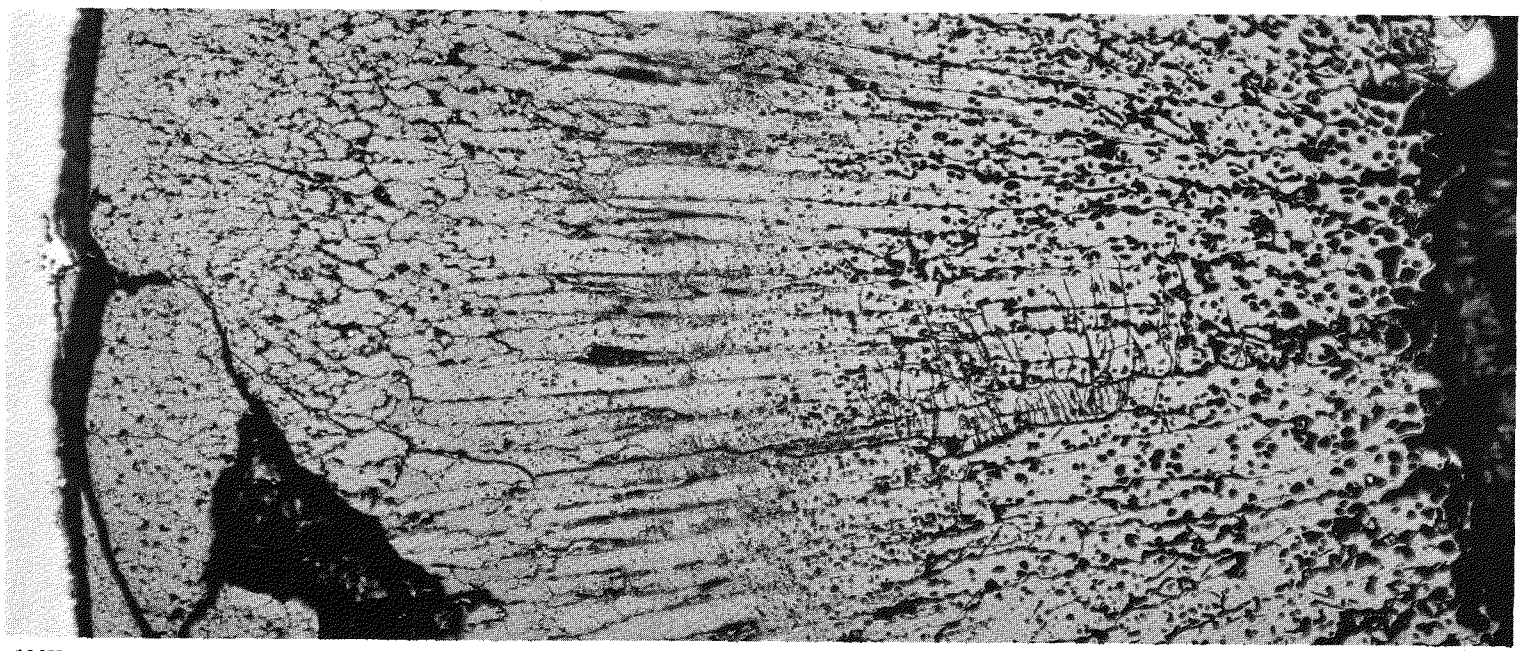

100X

HC16335 and HC16334

FIGURE 19. TRANSVERSE CROSS SECTION OF SPECIMEN 14 FROM CAPSULE BMI-44-2 SHOWING TYPICAL MICROSTRUCTURES OF SMALL EQUIAXED GRAINS AT THE EDGE FOLLOWED BY COLUMNAR GRAINS AND THEN LARGER EQUIAXED GRAINS AT THE MIDDLE OF THE SPECIMEN

The stringers running perpendicular to the columnar grains could not be identified.

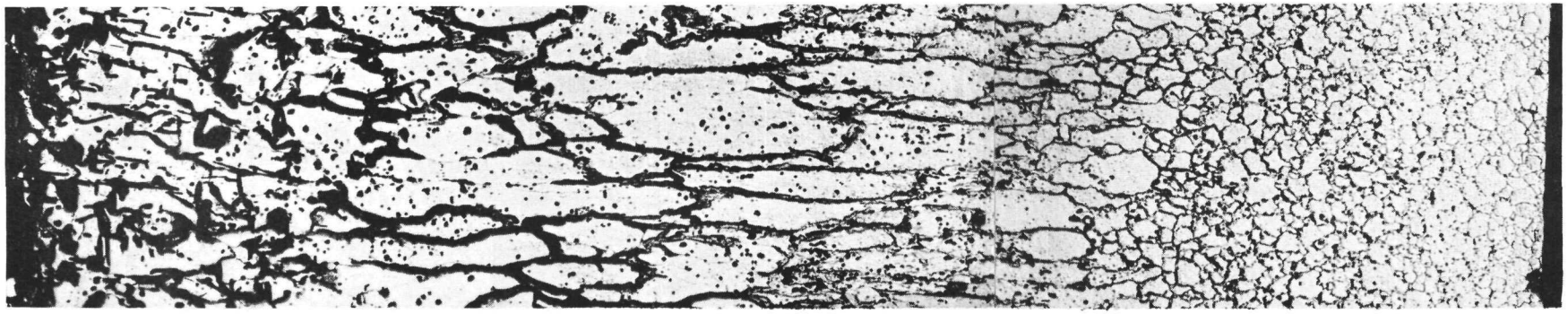

~100X

HC16316, HC16317 and HC16318

FIGURE 20. CROSS SECTION OF SPECIMEN 58 FROM CAPSULE BMI-44-4 SHOWING TYPICAL MICROSTRUCTURES OF SMALL EQUIAXED GRAINS AT THE EDGE FOLLOWED BY COLUMNAR GRAINS AND THEN LARGER EQUIAXED GRAINS NEAR THE CENTER OF THE SPECIMEN

Also note the thickening of grain boundaries.

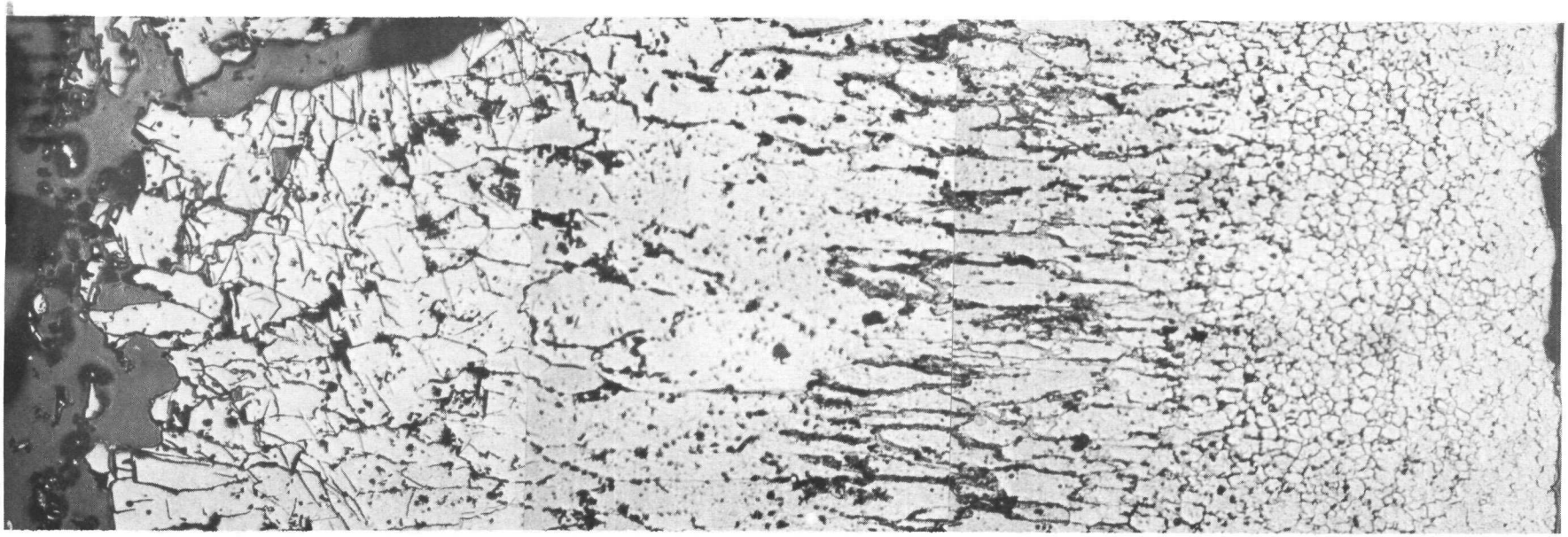

100X

HC15428, HC15429 and HC15430

FIGURE 21. CROSS SECTION OF SPECIMEN 35 FROM CAPSULE BMI-44-5 SHOWING THE TYPICAL MICROSTRUCTURE OF SMALL EQUIAXED GRAINS AT THE EDGE FOLLOWED BY COLUMNAR GRAINS AND THEN LARGER EQUIAXED GRAINS NEAR THE CENTER OF THE SPECIMEN.

Also note the thickening of grain boundaries.

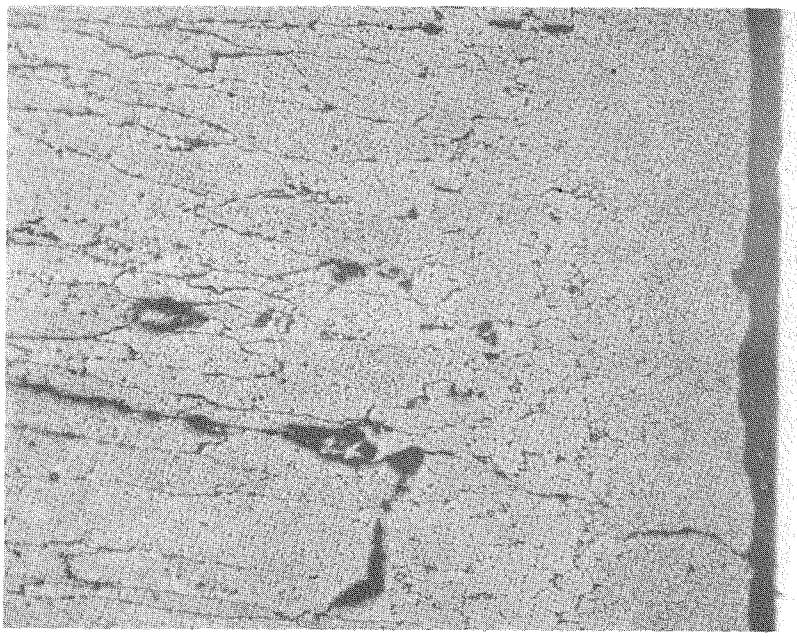

100X HC13864

a. Original Fuel

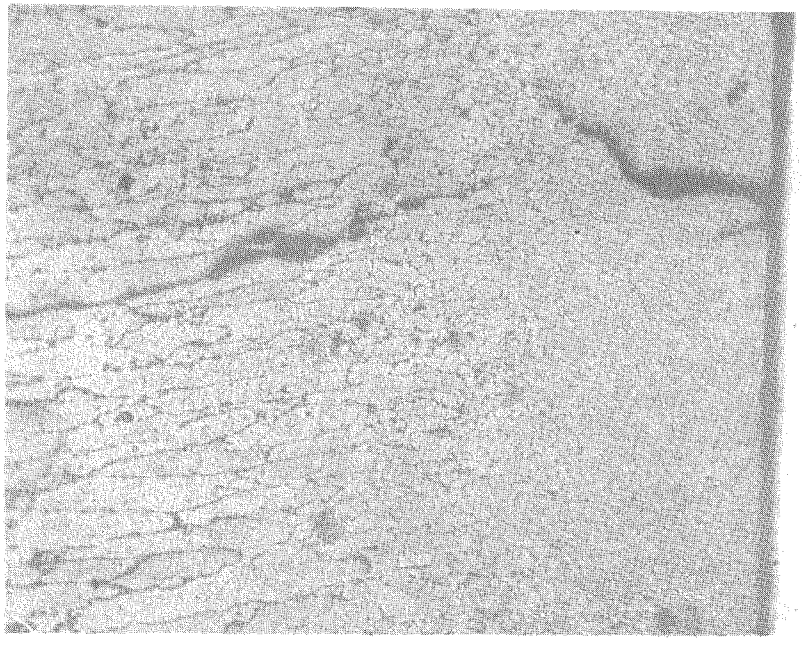

100X HC13863

b. Redeposited Fuel

FIGURE 22. MICROSTRUCTURE OF THE "ORIGINAL" AND "REDEPOSITED" UO_2 IN SPECIMEN 4 OF CAPSULE BMI-44-1

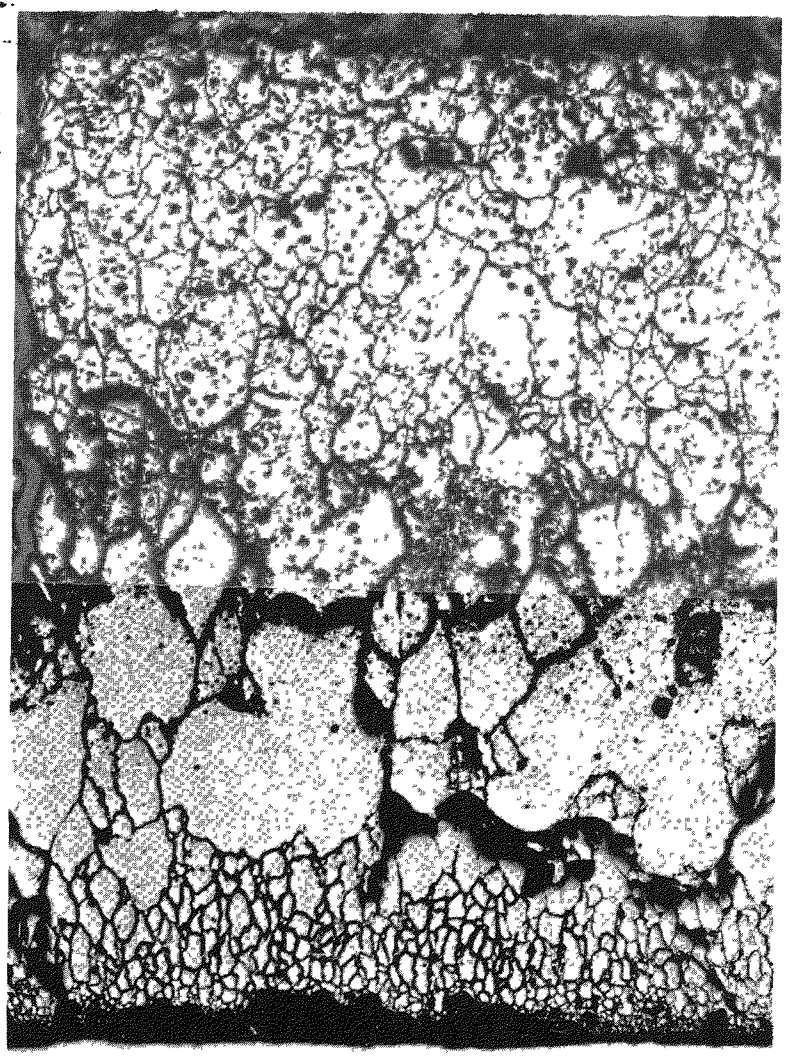

100X HC15460 and HC15461

a. Original Fuel

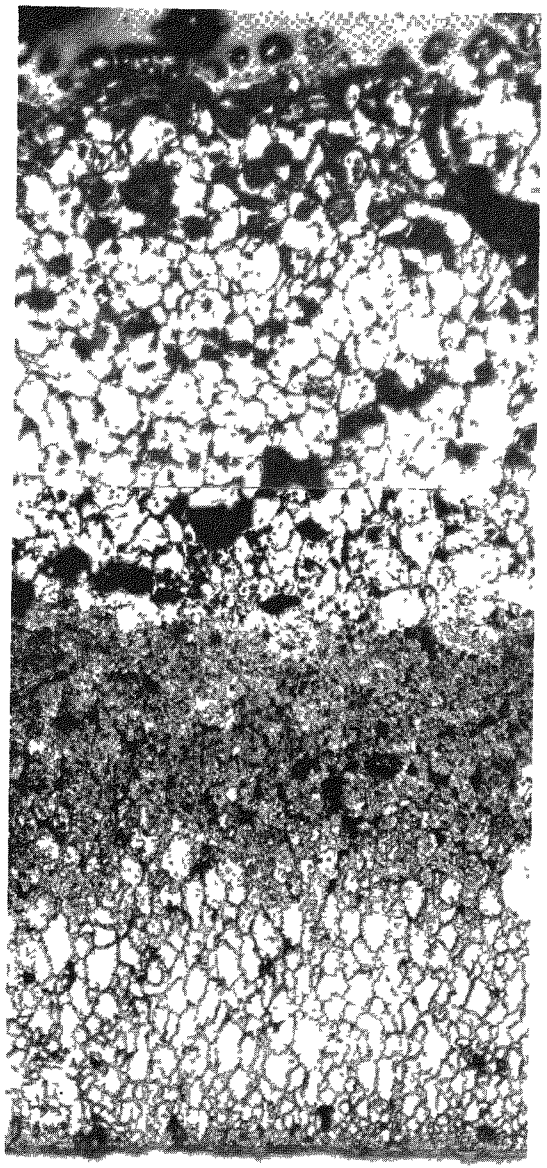

100X HC15469 and HC15470

b. Redeposited Fuel

FIGURE 23. MICROSTRUCTURE OF THE "ORIGINAL" AND "REDEPOSITED" UO_2 IN SPECIMEN 46 OF CAPSULE BMI-44-3
Also note the presence of white particles near the edge.

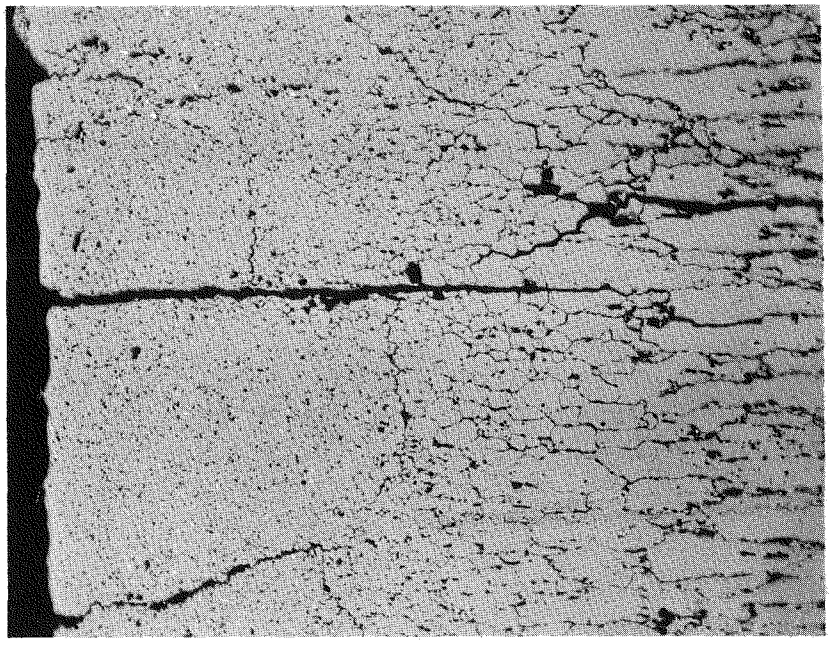

100X HC16319

a. Longitudinal Section of Specimen 58 from Capsule BMI-44-4

(3.3 a/o Burnup)

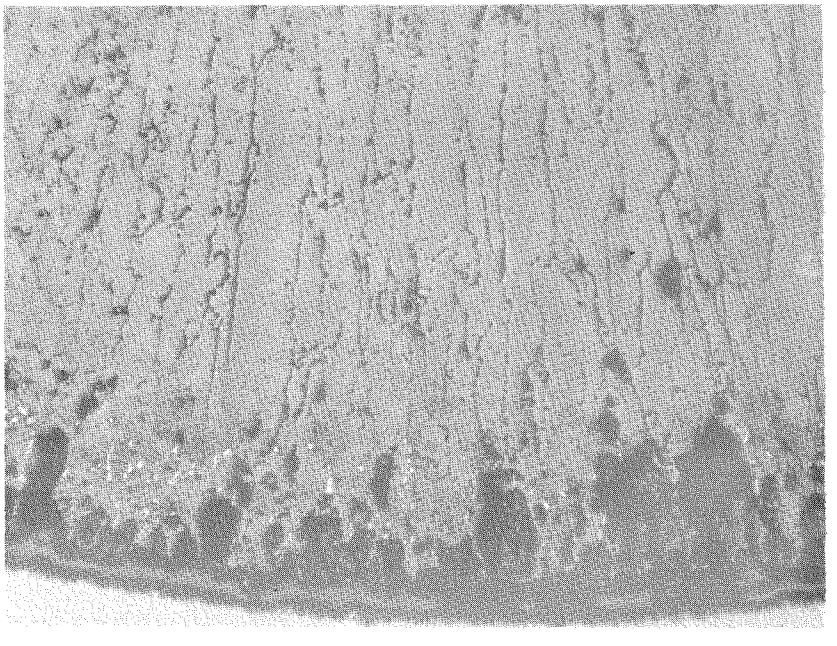

100X HC13880

b. Transverse section of Specimen 8 from Capsule BMI-44-1

(1.4 a/o Burnup)

FIGURE 24. PHOTOMICROGRAPHS SHOWING THE PRESENCE OF WHITE PARTICLES IN THE UO_2 NEAR THE CLADDING

The long crack in the above photograph (a) is a pellet interface. These particles are believed to be niobium rather than free uranium. Formation of the jagged edge is believed to result during sectioning of the specimen.

Therefore it seems likely that these white particles are refractory metals, either niobium or tungsten.

(5) There appears to be some thickening of grain boundaries with increased burnup. This is brought out by comparing Figures 22, 23, and 25. Similar grain-boundary thickening has been reported by other investigators.(7,8) This widening is believed to be caused by the accumulation of fission products at the grain boundaries.

(6) The grain boundaries of columnar grains found in the fuel etched considerably more severely than the grain boundaries of the equiaxed grains. After moderate etching, the fuel in some specimens fell out at the columnar grains. This is illustrated in Figures 23 and 26. This reaction is again believed to be due to concentration of fission products in the columnar grains generally, and in the grain boundaries of columnar grains particularly. Concentration of fission products in the columnar grains has been reported by other investigators.(9,10,11) The segregation of fission products at the grain boundaries seems to be a function of burnup, since the specimens irradiated to burnups of about 1.5 a/o of uranium do not show severe etching of the columnar grains.

(7) A minor reaction zone was found between the UO_2 fuel and the niobium-1 w/o zirconium cladding. This reaction zone was noticed in one specimen from Capsule BMI-44-1, which was in-pile for 1500 hr, and in one specimen each from Capsules BMI-44-4 and BMI-44-2 which were in-pile for 4900 and 5600 hr, respectively. It was not found in other specimens. In no instance was the depth of the reaction more than 1 mil thick. The reaction zone seems to be rather brittle since transverse cracks were found in it. Attempts were made to determine the microhardness of the reaction zone but the zone was too thin for the measurements. It was not possible to identify the reaction zone. The reaction zone is shown in Figure 27. Figures 19 through 26 show no reaction zone between the fuel and the cladding.

Microhardness measurements were taken across the claddings of various specimens to indicate any oxidation of the cladding. These measurements are given in Table 11 and show that only in one case, where the hardness of inside edge was 156, was there a possibility of oxidation or fission-product attack.

(8) The grain size of the niobium-1 w/o zirconium was increased considerably in a few specimens in the part of the cladding which was in contact with the lithium and adjacent to the fuel. The extreme case is illustrated in Figure 28. This is believed to be due to the removal of impurities by lithium from the cladding, which would allow recrystallization and grain growth to take place at lower temperatures. As shown in Figure 29, which compares the pre- and postirradiation structure, not all of the impurities were removed from the part of the cladding which was next to the void space at the

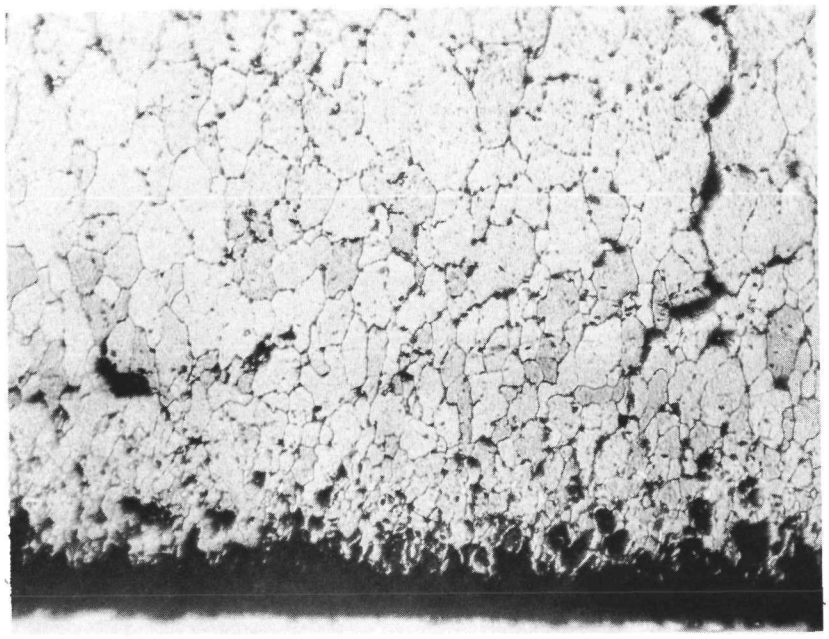

100X HC13850

a. Specimen 2 from Capsule BMI-44-1

(1.5 a/o Burnup)

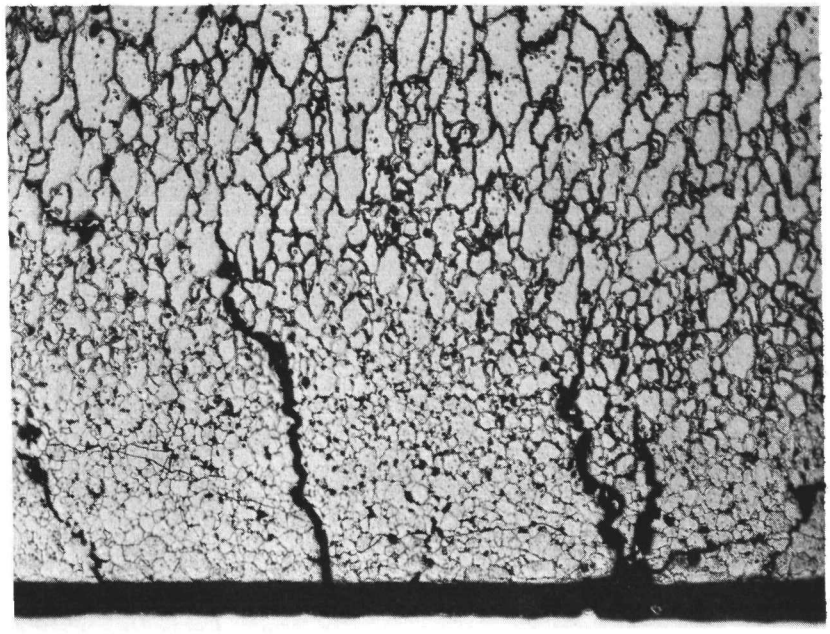

100X HC16295

b. Specimen 49 from Capsule BMI 44-4

(3.3 a/o Burnup)

FIGURE 25. PHOTOMICROGRAPHS SHOWING THE THICKENING OF GRAIN BOUNDARIES WHICH IS BELIEVED TO BE DUE TO CONCENTRATION OF FISSION PRODUCTS

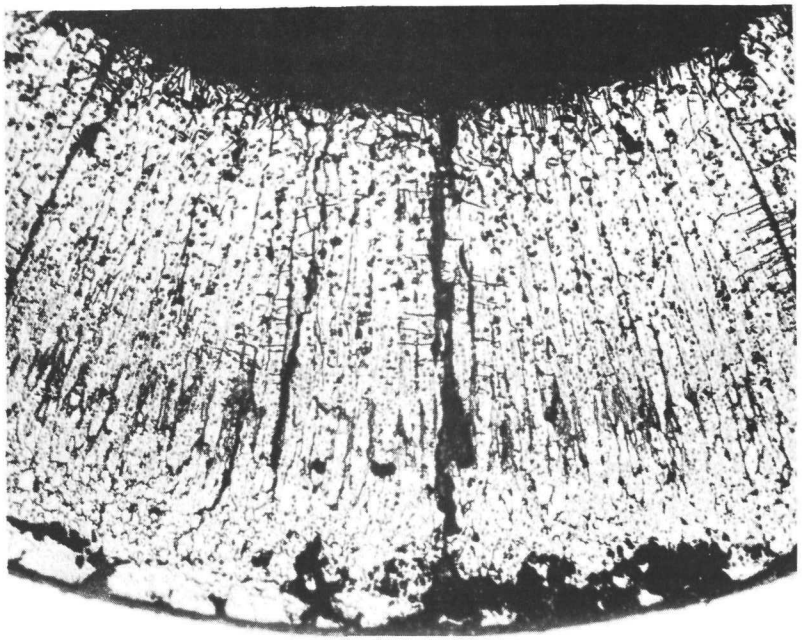

50X HC15439

a. Specimen 42 from Capsule BMI-44-3

(3.0 a/o Burnup)

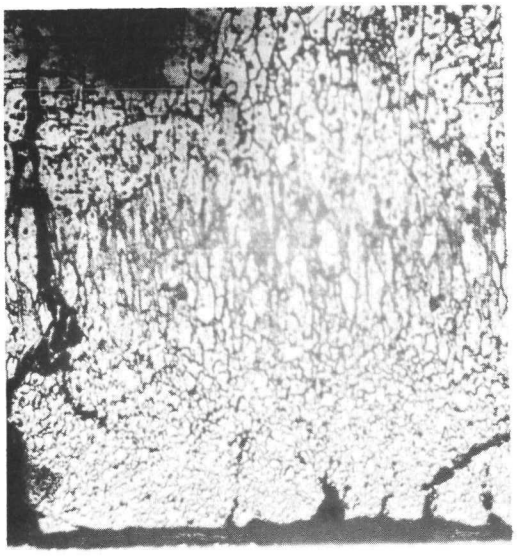

50X HC15390

b. Specimen 30 from Capsule BMI 44-5

(3.0 a/o Burnup)

50X HC13873

c. Specimen 4 from Capsule BMI 44-1

(1.4 a/o Burnup)

FIGURE 26. PHOTOMICROGRAPHS SHOWING THE SEVERE ETCHING OF GRAIN BOUNDARIES IN THE COLUMNAR GRAIN REGION

This is believed to be due to fission-product concentration in the columnar-grain region. This attack seems to increase with increased burnup in the UO_2.

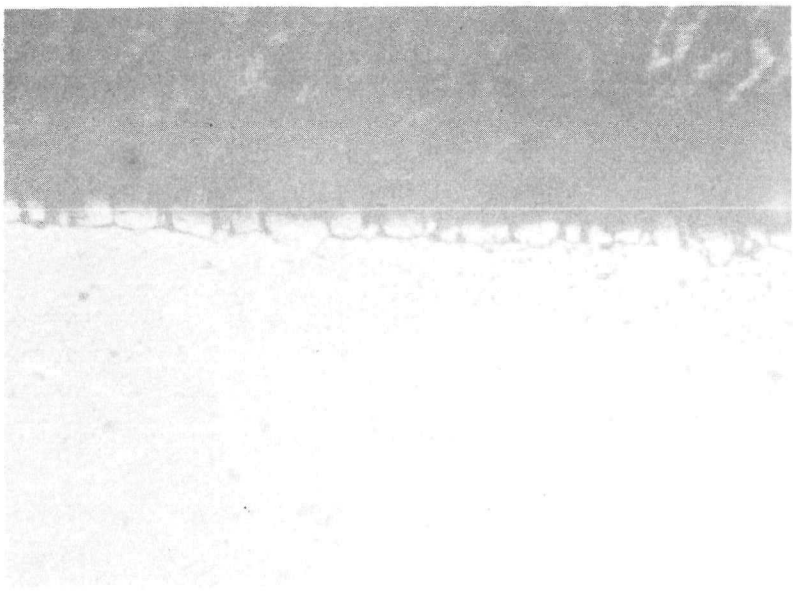

450X HC13878

a. 1500 Hr of Operation

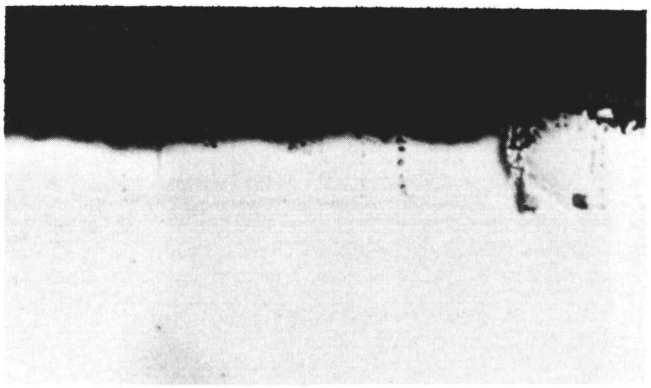

500X HC16315

b. 4900 Hr of Operation

250X HC16279

c. 5600 Hr of Operation

FIGURE 27. PHOTOMICROGRAPHS SHOWING A SMALL REACTION ZONE IN THE NIOBIUM-1 w/o ZIRCONIUM CLADDING

It was not possible to identify this reaction zone.

TABLE 11. MICROHARDNESS TRAVERSES ACROSS THE NIOBIUM-1 w/o ZIRCONIUM CLADDING

	Hardness, KHN					
	Unirradiated Control	Specimen 34	Specimen 36	Specimen 24	Specimen 45	Specimen 14
Inside Edge	116	83	82	156	110	101
	101	84	80	120	112	88
	102	83	80	100	100	116
	94	90	97	84	103	90
	93	90	100	82	89	104
	96	98	100	81	91	83
	97	94	98	84	83	73
	103	100	113	94	108	84
	90	98	101	94	116	80
	95	91	111	90	122	116
		98	121	88		
		97	115	90		
			124			
Outside Edge			100			

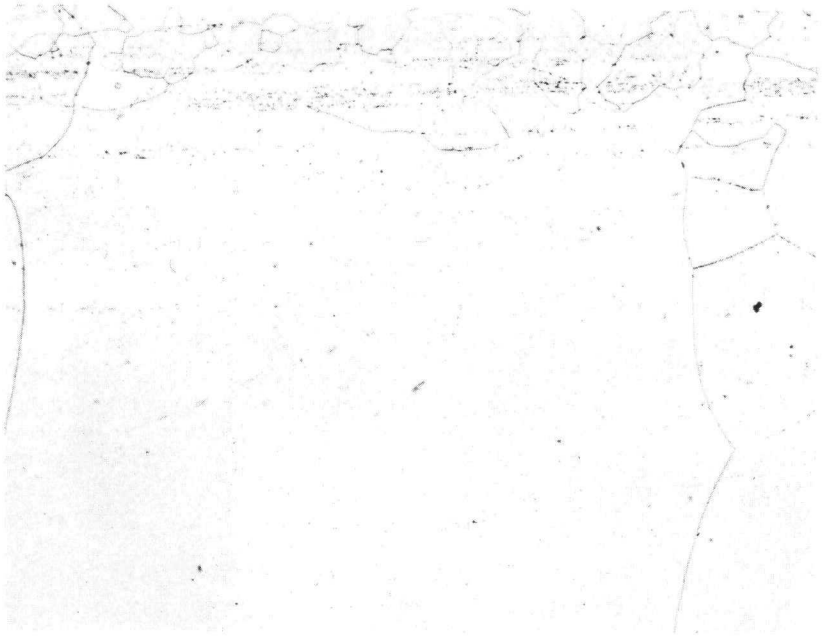

100X HC16272

a. Outer Surface of Cladding, Cladding in Contact With Fuel

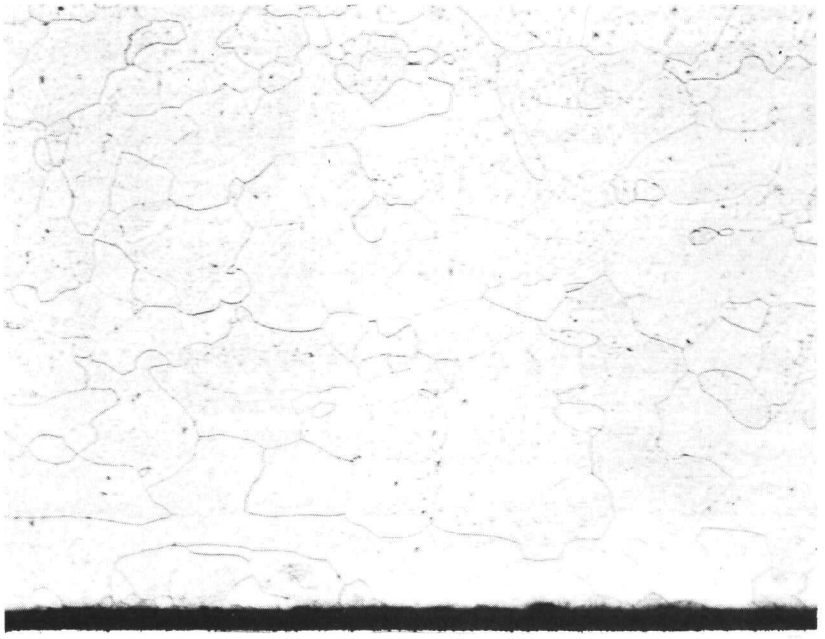

100X HC16270

b. Inner Surface of Cladding, Cladding in Contact With Fuel

FIGURE 28. PHOTOMICROGRAPHS SHOWING THE VARIATION OF GRAIN SIZE IN DIFFERENT LOCATIONS OF THE NIOBIUM-1 w/o ZIRCONIUM CLADDING

This difference is believed to be caused by removal of impurities from the cladding by lithium, thereby increasing the degree of grain growth at a specific temperature.

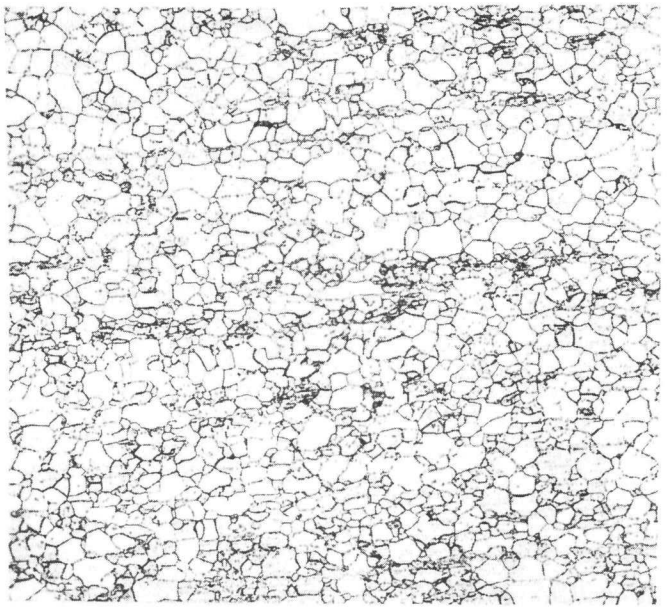

100X RM39037

a. Unirradiated

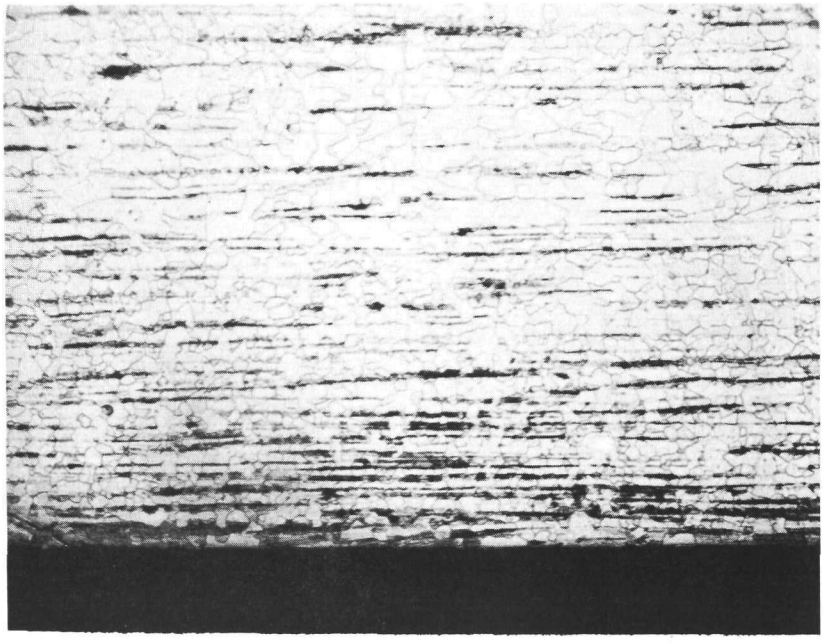

100X HC16268

b. Irradiated Cladding Next to Lithium but Not Next to the UO_2 Fuel

FIGURE 29. PHOTOMICROGRAPHS SHOWING THE STRUCTURE OF THE NIOBIUM-1 w/o ZIRCONIUM CLADDING BEFORE AND AFTER IRRADIATION

top of the specimen. This indicates that the temperature of the cladding in the upper part of the specimen was considerably lower than in the part of cladding adjacent to the fuel.

In most of the specimens some grain growth had taken place at either the outside or inside surface. This was found to be rather minimal when compared to the extreme case discussed above.

Oxygen/Uranium Ratio of UO_2

The oxygen/uranium ratio of the irradiated UO_2 was determined by polarographic techniques. Complete cross sections of fuel weighing about 1 g each were used as samples for these measurements. In determining the oxygen/uranium ratio by polarography, the UO_2 was dissolved in a mixture of phosphoric and sulfuric acids. Then an electric current was passed through the solution and a plot of voltage versus amperage was derived. This plot is compared with a plot from a control solution which contains known amounts of uranium with a +6 valence. By considering the amount of uranium with +6 valence and the weight of UO_2 in the sample, an oxygen/uranium ratio is determined.

It was found that the oxygen/uranium ratio increased with increased burnup as shown in Figure 30. The upward shift of the experimental curve from the theoretical curve is believed to be due to some factor in the experimental determinations in the hot cell, since the unirradiated controls which were analyzed in the hot cell also show an equal shift. Analyses performed on the unirradiated controls outside the hot cell gave oxygen/uranium ratios of 2.003. There is also a possibility that the presence of fission products in the irradiated UO_2 might shift the voltage versus current relationship in the polarographic determination of the oxygen/uranium ratios.

Although the oxygen/uranium ratio increase is believed to be due to further oxidation of UO_2 by the two oxygen atoms which are released when a uranium atom fissions, a survey of free energy of formation for the fission products at 1400 C showed that praseodymium, samarium, lanthanum, cerium, barium, strontium, neodymium, yttrium, promethium, europium, and gadolinium would form stable oxides at equilibrium conditions. All of the stable oxides would be in the form of sesquioxides except for Ba_2O and SrO. By taking into account the fission yields of the oxide-forming fission products it was calculated that 60 per cent of the released oxygen atoms would be used up in forming stable fission-product oxides in short-time irradiations. For long-term irradiations, the percentage of oxygen atoms taken up by stable fission-product oxides decreases to about 50 per cent because some of stable oxide fission products decay to nuclides which do not form stable oxides. This is further discussed in Appendix C.

Previous irradiations of hyperstoichiometric UO_2 have indicated comparatively poorer over-all performance than that for stoichiometric UO_2. The hyperstoichiometric UO_2 was found to have poorer thermal conductivity, higher fission-gas release, and poorer dimensional stability than stoichiometric UO_2.[12,13]

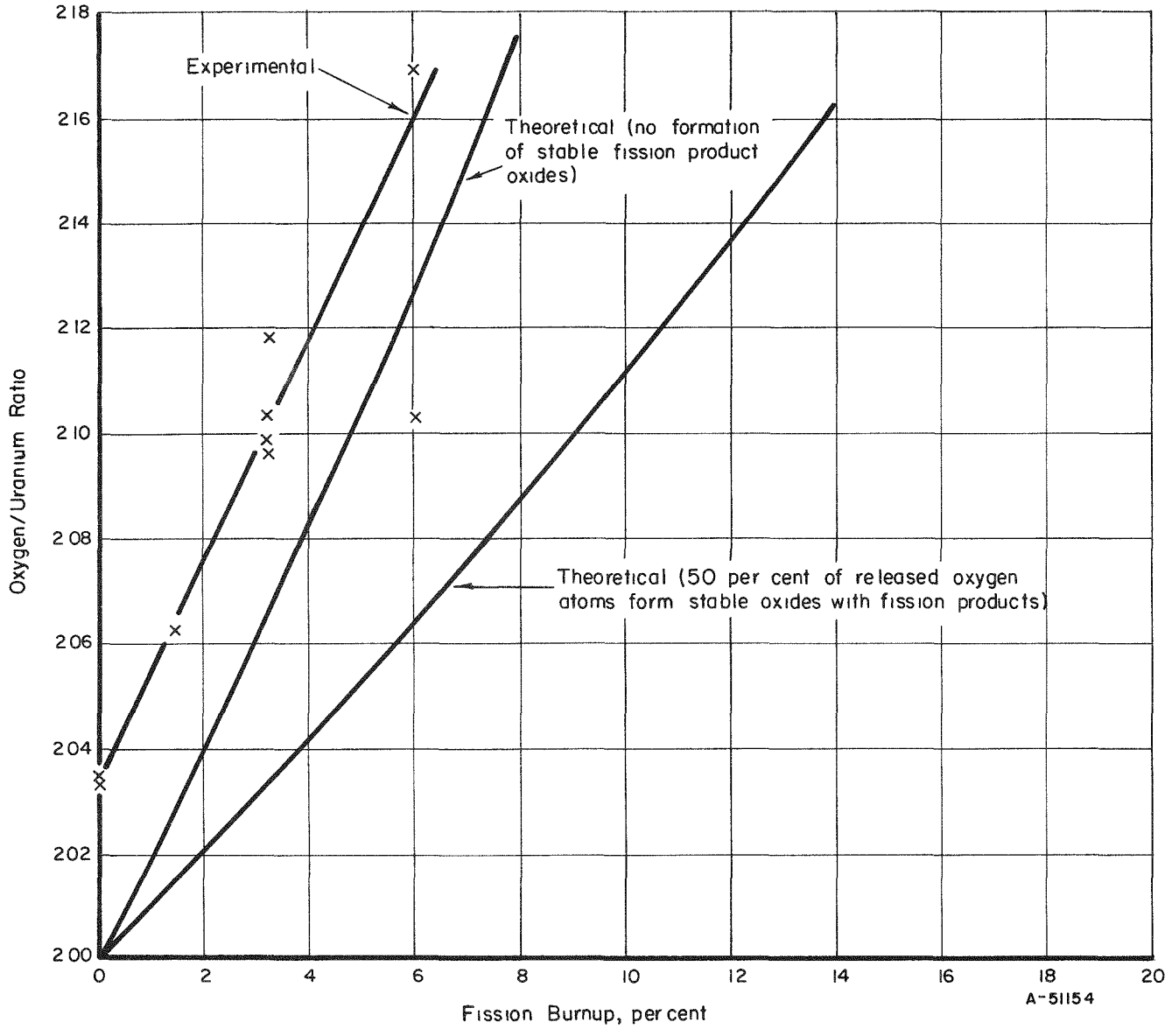

FIGURE 30. CHANGE IN THE OXYGEN/URANIUM RATIO OF UO_2 AS A FUNCTION OF BURNUP

The increase in the oxygen/uranium ratio with irradiation may be the explanation of high creep rates found in UO_2 during irradiation by Westinghouse investigators.[7] It has been found by Armstrong and Irvine[14] that the creep rate is very sensitive to increases in oxygen/uranium ratio. Also the increase in fission-gas release with burnup[15] may be caused, in part, by the increase in oxygen/uranium ratio during irradiation.

CONCLUSIONS

The following conclusions were derived from this study:

(1) Lithium and UO_2 are incompatible at 1100 C.

(2) No dimensional changes of the specimens took place because the heavy cladding was sufficient to withstand internal fission-gas pressure.

(3) A central void was formed in all specimens and fuel movement took place by a vaporization-redeposition mechanism. The vaporization rate was significantly reduced when the maximum fuel temperature decreased below 1900 to 2100 C.

(4) The size of the central void and the degree of the fuel movement were dependent on the initial central temperature and independent of burnup.

(5) The amount of fission gas released from the UO_2 ranged from 32 to 87 per cent, depending on the specimen surface temperature and the volume of fuel operating above 1600 C.

(6) Grain-boundary widening of the UO_2 took place at a burnup of above 2 to 3 a/o of uranium.

(7) White metallic particles found in the fuel are believed to be either tungsten or niobium.

(8) Minor reactions between the UO_2 and niobium-1 w/o zirconium were observed in some specimens. In all cases the reaction zone was less than 1 mil thick.

(9) The oxygen to uranium ratio of the UO_2 increased with increasing burnup.

(10) The UO_2 reached a stable configuration as a result of irradiation, with the configuration being dependent on specimen surface temperature and fissioning rate in the fuel.

REFERENCES

(1) Weidenbaum, B., "High Performance UO_2 Program", Quarterly Progress Reports, GEAP-3771-1 through -15 (July 1, 1961, through January 15, 1965).

(2) "Corrosion of Columbium-Base and Other Structural Alloys in High-Temperature Lithium", PWAC-355 (June 30, 1964). Confidential.

(3) Slorek, T. J., and Weidenbaum, B., "Fission Gases, Their Measurements and Evaluations", GEAP-3440 (August 15, 1960).

(4) Scott, J. L., "The Release of Kr^{85} from UO_2 in ORR Capsules", ORNL-3195 (October 6, 1961).

(5) Yunus, M., "The Recrystallization of UO_2 at High Temperatures", HW-tr-66 (1963).

(6) Bates, J. L., "Metallic Uranium in Irradiated UO_2", HW-82263 (May, 1964).

(7) Daniel, R. C., et al., "Effects of High Burnup on Zircaloy-Clad, Bulk UO_2, Plate Fuel Element Samples", WAPD-263 (September, 1962).

(8) Padden, T. R., and Schnizler, P. S., "Microstructural Changes Associated with Irradiation Burnup of UO_2", WAPD-T-1501 (August, 1962).

(9) Bates, J. L., et al., "Extensive Movement of Fission Fragments and Plutonium Demonstrated in UO_2 Irradiation Tests", HW-SA-2309 (October 6, 1961).

(10) Roake, W. E., "Irradiation Alteration of Uranium Oxide", HW-73072 (March, 1962).

(11) Morgan, W. W., et al., "A Preliminary Report on Radial Distribution of Fission-Product Xenon and Cerium in UO_2 Fuel Elements", CRDC-1027 (April, 1961).

(12) Ridal, A., et al., "Irradiation of Nonstoichiometric UO_2 for Short Durations", CRFD-994 (February, 1961).

(13) Robertson, J. A. L., "Concerning the Effects of Excess Oxygen in UO_2", CRFD-973 (October, 1960).

(14) Armstrong, W. M., and Irvine, W. R., "The Plastic Deformation of UO_2 at Elevated Temperatures", Paper presented at 63rd Annual Meeting of The American Ceramic Society, Toronto, 1961.

(15) Belle, J. (Editor), Uranium Dioxide: Properties and Nuclear Applications, Naval Reactors, Division of Reactor Development, USAEC (July, 1961).

MK:EGF:DHL:VWS:JEG/all

[redacted]

APPENDIX A

CLADDING DESIGN CRITERIA

UNCLASSIFIED

[redacted]

APPENDIX A

CLADDING DESIGN CRITERIA

The analyses leading to the design of the cladding for the specimens in the high-temperature UO_2 irradiation program are summarized in this Appendix. The specimens for four capsules had 0.225-in. diameters and a niobium-1 w/o zirconium cladding of 80 mils. The specimens for the one capsule had 0.29-in. diameters and a niobium-1 w/o zirconium cladding of 80 mils.

In designing the specimens, enough cladding strength was allowed to withstand the fission-product pressure built up inside the specimens at 1200 F. In considering the pressure buildup, all the volatile fission gases were taken into account. Since 2200 F is the lowest temperature in the specimens, all the fission products have boiling points lower than that temperature would be volatile. The fission products which are volatile and their fission yields are given in Table A-1.[1]* Barium and strontium would be volatile at this temperature, but their oxides are thermodynamically more stable than UO_2. Therefore, these fission products would reduce UO_2 to form Ba_2O and SrO.[2] The cesium and rubidium oxides are thermodynamically less stable than UO_2.

Various possibilities were considered which would prevent gaseous cesium and rubidium from exerting pressure on the specimen wall. One possibility was that cesium and rubidium would not vaporize at 1200 C because of the high gas pressure inside the specimens. Vapor-pressure data[3] indicate that the pressure would have to be considerably higher at 1200 C than was anticipated, to prevent cesium and rubidium from evaporating. The other possibility was that cesium and rubidium might react with the niobium-1 w/o zirconium cladding at 1200 C. Research at AGN has shown that no reaction occurs between rubidium and niobium-1 w/o zirconium at 990 C[4] and between cesium and niobium-1 w/o zirconium at 1010 C.[5] Therefore, it seems that there is little likelihood that any reaction would occur at 1200 C. No correction was made for possible cesium and rubidium diffusion into the cladding which would reduce the amount of cesium vapor available for contributing to the pressure. Therefore, a figure of 0.5 gas atom produced per fission allows a factor of safety.

In predicting fission-product release, the release of cesium and rubidium was taken as being equal to the release of xenon and krypton.[6] In calculating fission-product release from UO_2, the following method was used. The temperature profile of the capsule was determined by using the relationship

$$T_r = T_o + \frac{H}{4\pi k}\left[\frac{r_o^2 - r^2}{r_o^2}\right],$$

*References appear at end of Appendix.

TABLE A-1. VOLATILE FISSION PRODUCTS AT 2200 F

Isotope	Half-Life	Yield	
Br^{81}	Stable	0.14	
Kr^{83}	Stable	0.544	3.92
Kr^{84}	Stable	1.00	
Kr^{85}	10.3 y	0.36	
Kr^{86}	Stable	2.02	
Rb^{85}	Stable	0.94	3.43
Rb^{87}	6×10^{10} y	2.49	
I^{129}	1.7×10^{7} y	0.90	
Xe^{131}	Stable	2.93	19.83
Xe^{132}	Stable	4.38	
Xe^{134}	Stable	8.06	
Xe^{136}	Stable	6.46	
Ca^{133}	Stable	6.59	19.15
Ca^{135}	2.6×10^{6} y	6.41	
Ca^{137}	Stable	6.15	
		49.374	

where

r = distance from center, cm

r_o = radius of pellet, cm

T_r = temperature at distance r, C

T_o = temperature at surface, C

k = thermal conductivity (Chalk River Data)

H = heat flux, w per cm.

The diffusion parameter D' was used in these calculations where

$$\log D'_{1400} = -14.00 + 2 \log S \ ,$$

where S is the surface area of UO_2 in cm^2 per g.[7] The surface area was found to be 3.3 cm^2 per g for UO_2 with a theoretical density of 98 per cent.[8] The D' for other temperatures was determined from the relationship is:[7]

$$\ln \frac{D't}{D'_{1400}} = \frac{\Delta H}{R} \left[\frac{1}{1673} - \frac{1}{T + 273} \right] \ ,$$

where

ΔH = activation energy (A figure of 60 kcal per mole was chosen from values ranging from 45 to 115 kcal per mole.)

R = gas constant (1.987 cal per (g)(mole)(C).

The fractional fission-gas release at a given temperature is given by:

$$F = \frac{4}{\sqrt{\pi}} \sqrt{D'_T t} \ ,$$

where t is the time of irradiation in seconds.[7]

The fuel specimen was divided into concentric volumes and the average temperature for each volume was determined. By using the above equation, the fractional release from each volume was determined. The total fractional release for the whole specimen was then calculated and is given in Table A-2.

A uniform fissioning rate was assumed in these calculations. However, if flux perturbation was taken into account, the expected fission-gas release could be reduced by up to 25 per cent. The fission product pressure inside the specimens was calculated for the various specimens which had different fuel and void lengths. These values are given in Table A-2. The fission-gas temperature in the specimen voids was assumed to be 1095 C for the calculations.

TABLE A-2 DESIGN PARAMETERS FOR HIGH-TEMPERATURE UO_2 IRRADIATION PROGRAM

Capsule	No. of Specimens	Specimen Diameter, in	Fuel Length, in	Void Length, in	Burnup, a/o	Fractional Gas Release	Center Line Temperature, F	Clad Thickness, in.	Pressure Inside Specimens, psi	Maximum Stress[a], psi
1	6	0.225	0 75	1 05	1.5	0 74	4200	0.080	270	550
2	6	0.225	0.75	1 05	3 0	0.75	4200	0.080	530	1080
3	6	0 225	0.60	1 20	3 0	0 96	5000	0.080	480	975
4	6	0.290	0.75	1.05	3.0	0.76	4200	0.080	525	1275
5	6	0.225	0.60	1 20	5 0	0.77	4200	0.080	615	1250

(a) Calculated by using the stress formula $\text{stress} = \dfrac{\text{Inside Pressure } [(OD)^2 + (ID)^2]}{[(OD)^2 - (ID)^2]}$

In designing the specimens the maximum stress for thick-walled closed cylinders is:

$$\text{Stress} = \frac{\text{Inside Pressure } [(OD)^2 + (ID)^2]}{[(OD)^2 - (OD)^2]}$$

To prevent excessive creep from taking place in the cladding, the maximum stress was limited to 1200 psi. For a 1 per cent deformation by creep to take place at 1200 C. in niobium-1 w/o zirconium, a stress of 1300 psi for 5000 hr is needed.(9) Therefore, the stresses which are present in the specimens leave a considerable margin of safety even if a possible 15 per cent decrease in creep strength due to irradiation is considered.(10)

The above calculations indicate that the specimen claddings were designed with a large safety margin to minimize the possibility of contact between the lithium capsule coolant and UO_2. The safety margin resulted from:

(1) The design was based on a maximum stress during the whole irradiation, rather than on a continuously increasing stress with fission-product buildup which reaches the maximum at the end of the irradiation.

(2) A safety factor was left even when a 15 per cent decrease in strength, due to irradiation, was considered.

(3) Uniform fissioning throughout the fuel was considered. If flux perturbation due to high enrichment was taken into account, the fission-gas release would be reduced about 25 per cent.

References

(1) Belle, J., (Editor), Uranium Dioxide: Properties and Nuclear Applications, Naval Reactors, Division of Reactor Development, USAEC (July, 1961), p 478.

(2) Belle, J., (Editor), Uranium Dioxide: Properties and Nuclear Applications, Naval Reactors, Division of Reactor Development, USAEC (July, 1961), pp 548-49.

(3) Loftness, K. L., "A Vapor Pressure Chart for Metals" NAA-SR-132 (June 1, 1951).

(4) "Design and Operation of 1800°F Pumped Boiling Rubidium Loop System and Determination of Density and Vapor Pressure Between 174 and 1800°F", Final Report for Period February 1, 1960, through May 31, 1961, AGN-8034.

(5) "Cesium Corrosion and Thermo-Physical Properties Evaluation Program", Final Report for Period January 30, 1961, through February 15, 1962, AGN-8041, Confidential.

(6) Parker, G. W., "Fission Product Release from UO_2 by High Temperature Diffusion and Melting in Helium and Air", CF-60-12-14 (February 14, 1961).

(7) Scott, J. L., "The Release of Kr^{85} from UO_2 in ORR Capsules", ORNL-3195 (October 6, 1961).

(8) Eichenberg, J. D., et al., "Effects of Irradiation on Bulk UO_2", WAPD-183 (1957).

(9) "LCRE and SNAP 50-DR-1 Programs Engineering Progress Report", July 1, 1962 – September 30, 1962, PWAC-623 (October 31, 1962). Confidential.

(10) "Space Power Programs Semiannual Progress Report for Period Ending December 31, 1961", ORNL-3270. Secret.

[redacted]

APPENDIX B

BURNUP ANALYSIS

UNCLASSIFIED

[redacted]

BURNUP ANALYSIS

Equations Used for Burnup Determinations

(1) $100 \quad [1-R^{o}_{8/5}R_{5/8}]$

U^{238} not depleted

Independent of α

Best for high enrichment and high burnup

(2) $100 \left[\frac{R_{6/5} - R^{o}_{6/5}}{\frac{\alpha}{1+\alpha} + R_{6/5}}\right]$

U^{238} can be depleted

Must assume an α value, 0.185 used

Best for low enrichment and lower burnup

(3) $100 \left[\frac{(1+\alpha)(E^{o}_{5} - E_{5})}{E^{o}_{5}(1+\alpha - E_{5})}\right]$

U^{238} not depleted

Must assume as α value, 0.185; however, relatively insensitive to change in α.

Best for high enrichment and high burnup

Derivation of the Equations Used for Burnup on BMI Samples

I. $[1-R^{o}_{8/5}R_{5/8}]$

(1) $\frac{\text{g } U^{235} \text{ depleted}}{\text{g original } U^{235}} = \text{a/o } U^{235}$ depleted (when multiplied by 100) $= \frac{E^{o}_{5}U^{o} - E_{5}U}{E^{o}_{5}U^{o}} = 1 - \frac{E_{5}U}{E^{o}_{5}U^{o}}$

UNCLASSIFIED

(2) $E_8^o U^o = E_8 U$ Assume no loss of U^{238}

$$U/U^o = \frac{E_8^o}{E_8}$$

(3) $$1 - \frac{E_5 U}{E_5^o U^o} = 1 - \frac{E_5 E_8^o}{E_5^o E_8}$$ Substitute (2) into (3)

$$= 1 - R_{8/5}^o R_{5/8} .$$

II. $$\left[\frac{R_{6/5} - R_{6/5}^o}{\frac{\alpha}{1+\alpha} + R_{6/5}} \right]$$

(1) $$\alpha = \frac{E_6 U - E_6^o U^o}{E_5^o U^o + E_6^o U^o - E_5 U - E_6 U} = \frac{g\ U^{235}\ \text{captured}}{g\ U^{235}\ \text{fissioned}}$$

(2) $$1+\alpha = \frac{E_5^o U^o + E_6^o U^o - E_5 U - E_6 U + E_6 U - E_6^o U^o}{E_5^o U^o + E_6^o U^o - E_5 U - E_6 U}$$

$$= \frac{E_5^o U^o - E_5 U}{E_5^o U^o + E_6^o U^o - E_5 U - E_6 U}$$

(3) $$\frac{\alpha}{1+\alpha} = \frac{E_6 U - E_6^o U^o}{E_5^o U^o - E_5 U}$$

(4) $$\frac{\alpha}{1+\alpha} = \frac{E_6 U/U^o - E_6^o}{E_5^o - E_5 U/U^o}$$

(5) $$\alpha E_5^o - \alpha E_5 U/U^o = E_6 U/U^o - E_6^o + \alpha E_6 U/U^o - \alpha E_6^o$$

(6) $$\alpha E_6 U/U^o + E_6 U/U^o + \alpha E_5\ U/U^o = \alpha E_5^o + E_6^o + \alpha E_6^o$$

(7) $$U/U^o\ (\alpha E_6 + E_6 + \alpha E_5) = \alpha E_5^o + E_6^o + \alpha E_6^o$$

$$(8)\quad U/U^{o} = \frac{\alpha E_5^{o} + E_6^{o} + \alpha E_6^{o}}{\alpha E_6 + E_6 + \alpha E_5}$$

$$(9)\quad 1 - \frac{E_5 U}{E_5^{o} U^{o}} = 1 - \frac{\alpha E_5^{o} E_5 + E_5 E_6^{o} + \alpha E_5 E_6^{o}}{\alpha E_5^{o} E_6 + E_5^{o} E_6 + \alpha E_5^{o} E_5}$$

$$(10)\quad 1 - \frac{E_5 U}{E_5^{o} U^{o}} = \frac{\alpha E_5^{o} E_6 + E_5^{o} E_6 + \alpha E_5^{o} E_5 - \alpha E_5^{o} E_5 - E_5^{o} E_5 - E_5 E_6^{o} + \alpha E_5 E_6^{o}}{\alpha E_5^{o} E_6 + E_5^{o} E_6 + \alpha E_5^{o} E_5}$$

$$(11)\quad 1 - \frac{E_5 U}{E_5^{o} U^{o}} = \frac{\alpha E_5^{o} E_6 + E_5^{o} E_6 - E_5 E_6^{o} + \alpha E_5 E_6^{o}}{\alpha E_5^{o} E_6 + E_6^{o} E_6 + \alpha E_5^{o} E_5}$$

$$(12)\quad 1 - \frac{E_5 U}{E_5^{o} U^{o}} = \frac{\alpha \frac{E_6}{E_5} + \frac{E_6}{E_5} - \frac{E_6^{o}}{E_5^{o}} + \alpha \frac{E_6^{o}}{E_5^{o}}}{\alpha \frac{E_6}{E_5} + \frac{E_6}{E_5} + \alpha} \quad \text{divide by } E_5^{o} E_5$$

$$(13)\quad 1 - \frac{E_5 U}{E_5^{o} U^{o}} = \frac{\left[(1+\alpha)\frac{E_6}{E_5}\right] - \left[(1+\alpha)\frac{E_6^{o}}{E_5^{o}}\right]}{\alpha + (1+\alpha)\frac{E_6}{E_5}}$$

$$(14)\quad 1 - \frac{E_5 U}{E_5^{o} U^{o}} = \frac{\frac{E_6}{E_5} - \frac{E_6}{E_5^{o}}}{\frac{\alpha}{1+\alpha} + \frac{E_6}{E_5}} \quad \text{divide by } 1 + \alpha$$

UNCLASSIFIED

(15) $$1 - \frac{E_5 U}{E_5^o U^o} = \frac{R_{6/5} - R^o_{6/5}}{\frac{\alpha}{1+\alpha} + R_{6/5}}$$

III. $$\left[\frac{(1+\alpha)\ (E_5^o - E_5)}{E_5^o\ (1 + \alpha - E_5)} \right]$$

(1) $E_5^o U^o - E_5 U = 1 + \alpha\ (U^o - U)$ Assume no loss of U^{238}

(2) $E_5^o = E_5 U/U^o + (1+\alpha)\ (1 - U/U^o)$

(3) $E_5^o = E_5 U/U^o + 1 - U/U^o + \alpha - \alpha\ U/U^o$

(4) $E_5^o - 1 - \alpha = U/U^o\ (E_5 - 1 - \alpha)$

(5) $$U/U^o = \frac{E_5^o - 1 - \alpha}{E_5 - 1 - \alpha} = \frac{1 + \alpha - E_5^o}{1 + \alpha - E_5}$$

(6) $$\frac{E_5 U}{E_5^o U^o} = \frac{E_5\ (1 + \alpha - E_5^o)}{E_5^o\ (1 + \alpha - E_5)}$$

(7) $$1 - \frac{E_5 U}{E_5^o U^o} = 1 - \frac{E_5\ (1 + \alpha - E_5^o)}{E_5^o\ (1 + \alpha - E_5)}$$

$$= \frac{E_5^o + \alpha E_5^o - E_5^o E_5 - E_5 - \alpha E_5 + E_5^o E_5}{E_5^o\ (1 + \alpha - E_5)}$$

$$= \frac{E_5^o + \alpha\ E_5^o - E_5 - \alpha\ E_5}{E_5^o\ (1 + \alpha - E_5)}$$

$$(7)\quad 1 - \frac{E_5 U}{E_5^o U^o} = \frac{\alpha (E_5^o - E_5) + (E_5^o - E_5)}{E_5^o (1 + \alpha - E_5)}$$

$$= \frac{(1 + \alpha)(E_5^o - E_5)}{E_5^o (1 + \alpha - E_5)}$$

BLANK

[redacted]

APPENDIX C

FISSION-PRODUCT-OXIDE FORMATION

UNCLASSIFIED

[redacted]

APPENDIX C

FISSION-PRODUCT-OXIDE FORMATION

For every uranium atom that fissions, the following distribution of oxide-forming fission products would be found after 100 days.

Isotope	Fraction of Fission Product Present(1)*	Stable Oxide Formed(2-5)	Oxygen Atoms Taken Up
Sr^{88}	0.0370	SrO	0.0370
Sr^{89}	0.0271	SrO	0.0271
Sr^{90}	0.0590	SrO	0.0590
Y^{89}	0.0209	Y_2O_3	0.0315
Y^{91}	0.0344	Y_2O_3	0.516
Ba^{138}	0.0580	Ba_2O	0.0290
La^{139}	0.0600	La_2O_3	0.0900
Ce^{140}	0.0630	Ce_2O_3	0.0945
Ce^{141}	0.0367	Ce_2O_3	0.0550
Ce^{142}	0.0590	Ce_2O_3	0.0885
Ce^{144}	0.0610	Ce_2O_3	0.0915
Pr^{141}	0.0233	Pr_2O_3	0.0350
Nd^{143}	0.0620	Nd_2O_3	0.0930
Nd^{145}	0.0420	Nd_2O_3	0.0630
Nd^{146}	0.0330	Nd_2O_3	0.0495
Nd^{148}	0.0180	Nd_2O_3	0.0270
Nd^{150}	0.0074	Nd_2O_3	0.0111
Sm^{149}	0.0130	Sm_2O_3	0.0195
Sm^{151}	0.0050	Sm_2O_3	0.0075
Sm^{152}	0.0030	Sm_2O_3	0.0045
Sm^{154}	0.0009	Sm_2O_3	0.0013
Pm^{147}	0.0260	Pm_2O_3	0.0390
Eu^{153}	0.0015	Eu_2O_3	0.0022
Eu^{155}	0.0003		0.0005
Therefore: 50 per cent of available oxygen atoms are taken up by stable fission-product oxides.			1.0072

*References listed on following page.

References

(1) Blomeke, J. O., and Todd, M. F., "Uranium-235 Fission-Product Production as a Function of Thermal Neutron Flux, Irradiation Time, and Decay Time", ORNL-2127, Part 1, August 19, 1957.

(2) Coughlin, J. P., "Contributions to the Data on Theoretical Metallurgy, XII. Heats and Free Energies of Formation of Inorganic Oxides", Bureau of Mines Bulletin 542, U. S. Government Printing Office (1954).

(3) Glassner, A., "The Thermochemical Properties of the Oxides, Fluorides, and Chlorides to 2500 K", ANL-5750 (No date).

(4) Elliott, J. F., and Gleiser, M., Thermochemistry for Steelmaking, Volume I, Addison-Wesley Publishing Company, Inc., Reading, Massachusetts (1960).

(5) Dergazarien, T. E., et al., "JANAF Interin Thermochemical Tables", Volumes I and II, Joint Army, Navy, and Air Force Publication (December, 1960).